Geochemistry, Zircon U–Pb Dating and Hf Isotopic Characteristics of Neoproterozoic Granitoids in the Yaganbuyang Area, Altyn Tagh, NW China

CHEN Hongjie[1, 2, 3], WANG Nan[4, *], WU Cailai[1], LEI Min[1], ZHENG Kun[1], ZHANG Xin[1] and GAO Dong[1]

1 *Centre for Continental Dynamics, China Geological Survey, Institute of Geology, Chinese Academy of Geological Sciences, Beijing 100037, China*
2 *China University of Geosciences, Beijing 100083, China*
3 *Zhengzhou Normal University, College of Geography and Tourism, Zhengzhou 450044, China*
4 *MLR Key Laboratory of Metallogeny and Mineral Assessment, Institute of Mineral Resources, Chinese Academy of Geological Sciences, Beijing 10037, China*

Abstract: The South Altyn continental block is an important geological unit of the Altyn Tagh orogenic belt, in which numerous Neoproterozoic granitoids crop out. Granitoids are mainly located in the Paxialayidang–Yaganbuyang area and can provide indispensable information on the dynamics of Rodinia supercontinent aggregation during the Neoproterozoic. Therefore, the study of granitoids can help us understand the formation and evolutionary history of the Altyn Tagh orogenic belt. In this work, we investigated the Yaganbuyang granitic pluton through petrography, geochemistry, zircon U–Pb chronology, and Hf isotope approaches. We obtained the following conclusions: (1) Yaganbuyang granitoids mainly consist of two-mica granite and granodiorite. Geochemical data suggested that these granitoids are peraluminous calc–alkaline or high-K calc–alkaline granite types. Zircon U–Pb data yielded ages of 939±7.1 Ma for granodiorite and ~954 Ma for granitoids, respectively. (2) The $\varepsilon_{Hf}(t)$ values of two–mica granite and granodiorite are in the range of −3.93 to +5.30 and −8.64 to +5.19, respectively. The Hf model ages (T_{DM2}) of two-mica granite and granodiorite range from 1.59–.05 Ga and 1.62–2.35 Ga, respectively, indicating that the parental magma of these materials is derived from ancient crust with a portion of juvenile crust. (3) Granitoids formed in a collisional orogen setting, which may be a response to Rodinia supercontinent convergence during the Neoproterozoic.

Key words: granites, geochemistry, U–Pb dating, Hf isotopic characteristics, Altyn Tagh orogen belt

1 Introduction

Granitoids provide important information for reconstructing the history of orogenic belts. Various theories and genetic models have been proposed, reflecting different petrogenetic mechanisms (Bonin, 2007; Milani et al., 2015; Wang et al., 2018). Large-scale granitic batholiths develop during different orogenic evolutionary stages, particularly during the oceanic subduction or continental collision. Syn-collisional granitic magmatism occurs through the partial melting of the continental crust induced by continental collision and plays an important role in orogenic evolution and crustal growth (Zhao et al., 2017). Various products of syn-collisional magmatism, such as adakites, low Sr/Y sodic lavas, tonalites, and S-type granites, exist (Song et al., 2015).

During continental collision, the thickened crust undergoes temperature increases and evolves in accordance with clockwise pressure–temperature paths where liquidus temperatures are reached and partial melting occurs (Brown, 1993, 2001). Continental collisional events usually result in the juxtaposition of several unrelated rock units (Agyei–Dwarko et al., 2012). Rock units that record ancient orogenic events are invariably overprinted by those that record a series of later

* Corresponding author. E-mail: wangnan_0912@sina.com

orogenic events. Recent geochronological data indicates that the Altyn–Qilian–North Qaidam region has experienced Neoproterozoic (800 to 1000 Ma) magmatism and metamorphism related to Grenville orogenesis and the formation of the Rodinia supercontinent (Lu et al., 1998; Guo et al., 1999; Mei et al., 1999; Chen et al., 2006; Wan et al., 2006; Yu et al., 2013a, b; Wang et al., 2013; Li et al., 2015; Wang et al., 2015). However, given that prior geologic information has been obliterated during early Paleozoic orogeny, crust evolution during the Mesoproterozoic to early Neoproterozoic is unclear, and its potential information remains poorly explored. The nature and distribution of Neoproterozoic tectothermal events and their relationship with Grenville orogenesis and the Rodinia supercontinent have not been well defined.

In this paper, we present the systematic analyses of whole-rock elements, zircon U–Pb, and Hf isotopes of the Yaganbuyang pluton. The emplacement time of the pluton between 954 and 939 Ma provides evidence that it originates from syn-collisional-related magmatic rocks. These results provide new insights into Neoproterozoic crustal reworking in response to syn-collision in Altyn Tagh.

2 Geological Background

The NEE-trending, strike-slip Altyn Tagh Fault is the largest fault in Asia and defines the northern boundary of the Qinghai–Tibet Plateau. In accordance with the petrology, geochemistry and isotopic chronological characteristics of the different geological units of the orogenic belt, the Altyn Tagh orogenic belt can be divided into the Northern Altyn metamorphic terrane, North Altyn subduction accretionary complex belt, Meso–Neoproterozoic Central Altyn tectonic belt, Southwest Altyn subduction–collision complex belt, and South Altyn mafic-ultramafic rock belt (SAB) (Fig. 1) (Xu et al., 1999; Liu et al., 2009a, 2009b, 2012; Wu et al., 2009, 2014, 2016). Previous studies have shown that the Altyn Tagh orogenic belt was formed during the Archean and subsequently experienced intensive alterations through multiple magma–tectonic thermal events/collision orogeny during the Paleoproterozoic and Neoproterozoic (Che et al., 1995; Liu et al., 2009b) and subduction–collision between ancient blocks during the early Paleozoic (Liu et al., 1996; 1999; Xu et al., 1999; Zhang et al., 1999, 2001; Cui et al., 2011).

Granitic rocks exposed in the SAB mainly belong to the Altyn Group and are composed of metamorphic complexes, including tonalitic–granodioritic gneisses, sillimanite gneisses, kyanite garnet gneisses, and garnet amphibolite (Yu et al., 2002; Zhang et al., 2011). South Altyn HP and UHP metamorphic rocks mainly consist of garnet lherzolite, eclogite, granulite, and amphibole eclogite and occur mainly in the Jianggalesayi, Yinggelisayi, and Danshuiquan areas (Wang et al., 2013; Yu et al., 2011; Liu et al., 2016). These rocks have metamorphic ages of 509–475 Ma, which indicate that the continental crust deeply subducted under the oceanic crust during the late Cambrian–early Ordovician (Zhang et al. 1999, 2004; Liu et al. 2007a, 2007b; Cao et al., 2009). Recently, the Neoproterozoic ages of protoliths from HP/UHP metamorphic rocks have been obtained (Liu et al., 2009a; Wang et al., 2011) and demonstrated that at least some of the protoliths formed during the Neoproterozoic. Wang et al. (2006) reported that syn-collisional granitic gneiss from the Altyn Group has an age of 923±13 Ma. In addition, various U–Pb zircon ages (920–940 Ma) for the granitoid rocks of the Altyn Group have been reported (Zhang et al., 2011). These data suggested that the Altyn Complex may represent a Neoproterozoic piece along the southeastern margin of the Tarim craton (Wang et al. 2013).

3 Sampling and Petrography

The Neoproterozoic granitic intrusive rocks of the Altyn Tagh orogenic belt are mainly distributed in the Yaganbuyang–Paxialayi area and intrude into the metamorphic Proterozoic supracrustal rocks of the Altyn Group. Neoproterozoic granitoids in this area can be divided into the Gailike and the Yagabuyang pluton units on the basis of pluton formation age, rock types, and intrusive relationships (Li et al., 2015).

The Yaganbuyang pluton in the Suwushijie area is elongated along the EW direction. The pluton is off-white–gray in color and is medium-grained in texture (Fig. 2a) with a few feldspar phenocrysts. It presents globularly weathered and gneissic features (Fig. 2b) with intensive plastic deformation and local mylonitization. Amphibolite, mica schist xenolith, darkly colored schlieren and quartz, and pegmatite veins can be identified in the pluton (Fig. 2c). Field outcrop observation integrated with indoor microscopic analysis revealed that Yaganbuyang granitoids predominantly consist of two-mica granite (Fig. 2a) and granodiorite (Fig. 2b). We posited that, given the lack of obvious contact between the two-mica granite and granodiorite, a gradual transition relationship exists between these two types of rocks. The two-mica granite has an off-white in color, a granular squama crystal in texture with medium grains, and an oriented structure. It is composed of plagioclase (20%–25%), quartz (25%–30%), K-feldspar (30%–35%), biotite (3%–5%), and muscovite (8%–10%) (Fig. 2d). Granodiorite is off-white in color,

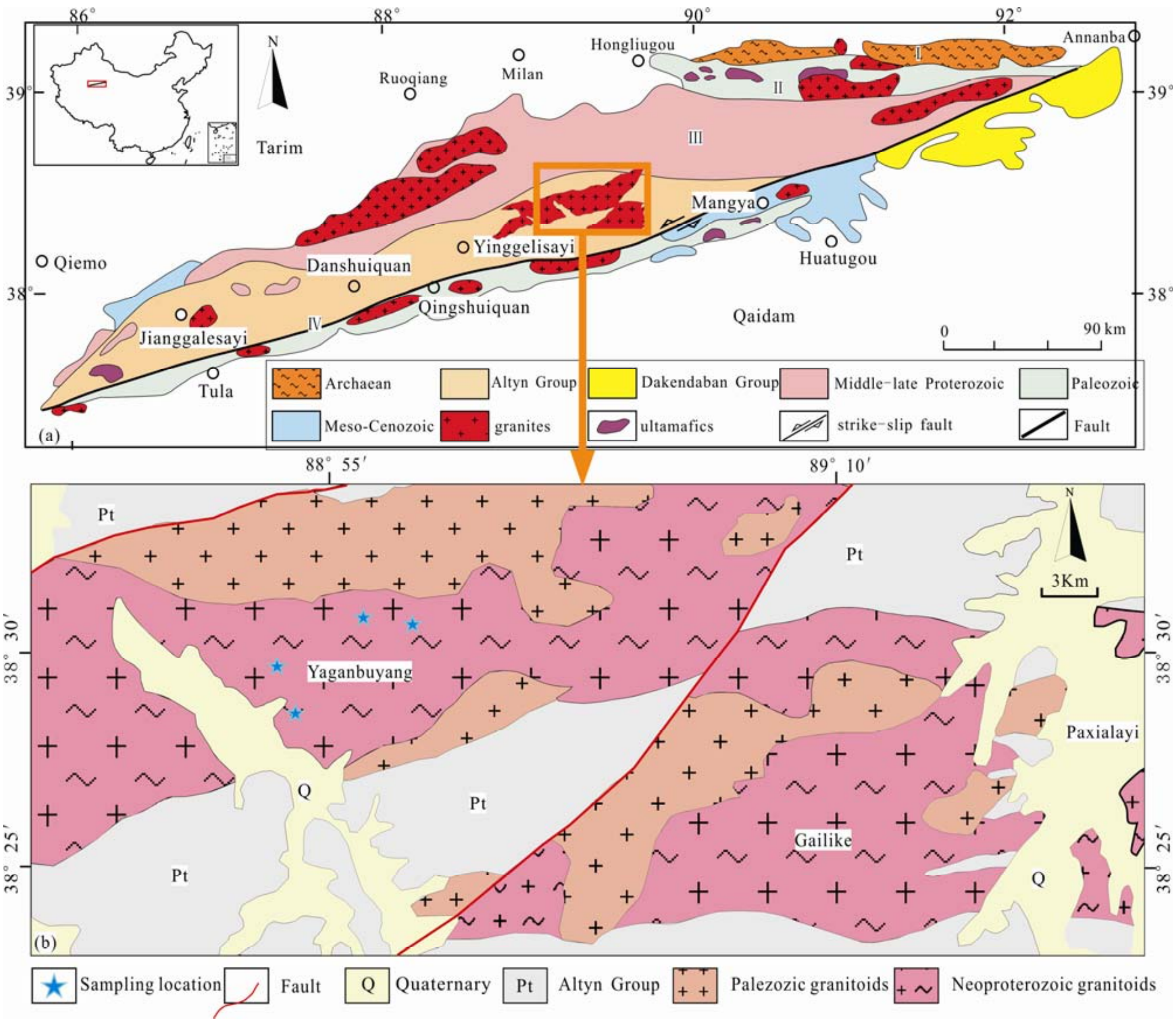

Fig. 1. (a) geological sketch map of Altyn Tagh orogenic belt （China basemap after China National Bureau of Surveying and Mapping Geographical Information); (b), geological sketch map of study area (a, after Wu Cailai et al., 2016; b, after 1:250,000 geological map of Suwushijie).

I, NAB (Northern Altyn metamorphic terrane); II, NAB (North Altyn subduction accretionary complex belt); III, CAB (Meso– Neoproterozoic Central Altyn tectonic belt); IV, SAB (Southwest Altyn subduction–collision complex belt, South Altyn mafic–ultramafic rock belt).

medium-grained, and granoblastic in texture with intensive transformation. It is composed of plagioclase (35%–45%), quartz (20%–25%), K-feldspar (13%–15%), and biotite (10%–15%) (Fig. 2e).

4 Analytical Methods

4.1 Whole–rock geochemistry

Eight samples were subjected to whole-rock chemical analyses at the Hebei Institute of Regional Geological and Mineral Resource Survey, Langfang, Hebei Province, China. Oxide concentrations were measured using a 3080E X–ray fluorescence spectrometer. Na_2O, MgO, Al_2O_3, SiO_2, P_2O_5, K_2O, CaO, TiO_2, MnO, Fe_2O_3 and FeO concentrations were analyzed in accordance with the executive standard GB/T14506.28–1993; H_2O^+ and CO_2 concentrations were analyzed in accordance with GB/T14506.2–1993 and GB9835–1988, respectively; and LOI was analyzed in accordance with LY/T1253–1999. The relative standard deviations were lower than 2%–8%. Rare earth (REEs; La, Ce, Pr, Nd, Sm, Eu, Gd, Tb, Dy, Ho, Er, Tm, Yb, Lu, and Y) and trace elements (Cu, Pb, Hf, Ta, Sc, Cs, V, Co, and Ni) were measured through ICP–MS (PlasmaQuad Excell) with JY/T016–1996 as the executive standard. The analytical precision of most elements was 10^{-8}, except for Zr and Ba (10^{-6}) and Hf and Nb (10^{-7}). The relative standard deviation was less than 10%. Analytical results are listed in Table 1.

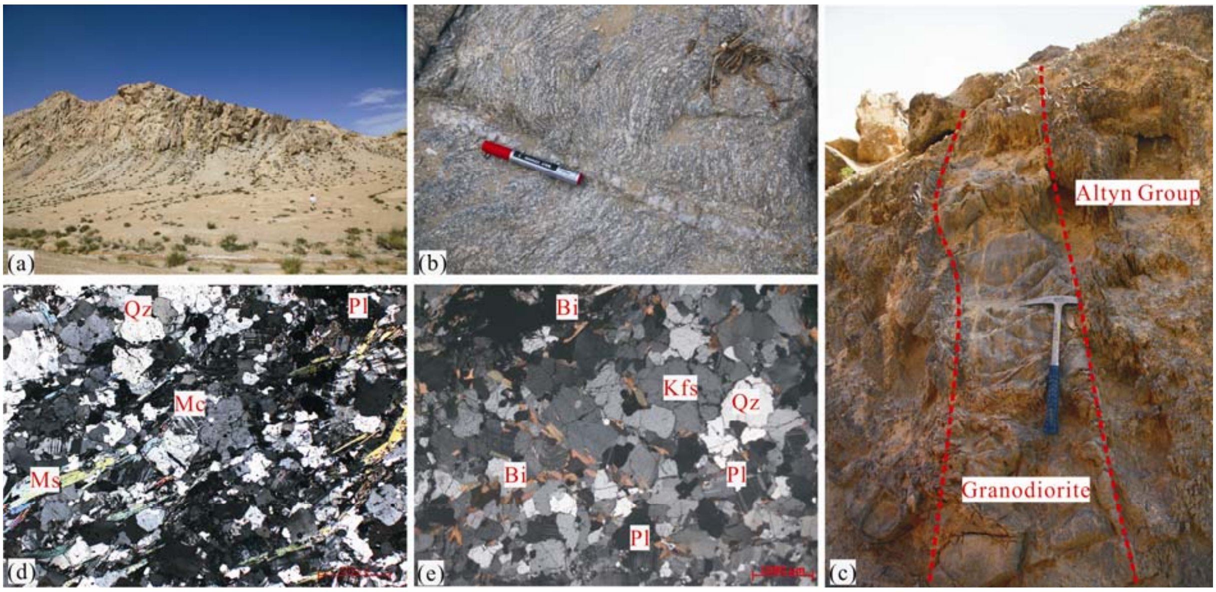

Fig. 2. Outcrops and Photomicrographs of Yaganbuyang pluton.
(a), Outcrop of Yaganbuyang two–mica granite; (b), photograph of Yaganbuyang granodiorite; (c) granodiorite dike intruded into metamorphic supracrustal rock of the Altyn Group; (d), photomicrograph of two–mica granite (Cross polarizer); (e), photomicrograph of granodiorite (Cross polarizer); Pl—plagioclase; Mc—microcline; Qz—quartz; Bi—biotite; Ms—muscovite; (after Whiney and Evans, 2010).

4.2 Zircon U–Pb dating

U, Th, and Pb analyses of zircons were performed on a LA–MC–ICP–MS apparatus at the Institute of Geology, Chinese Academy of Geological Sciences, following the procedures described by Hou et al., (2009). Spot sizes were ~32 μm, and data were calibrated to the M127 reference zircon (U: 923 ppm; Th: 439 ppm; Th/U: 0.475, Nasdala et al., 2008). Standard zircon was analyzed first, and analysis was repeated after every five spots. GJ-1 zircon with an age of 599.8±1.7 Ma (2σ) (Jackson et al., 2004) and Plesovice zircon with an age of 337.13±0.37 Ma (2σ) (Sla´ma et al., 2008) were used as reference standards. The ICPMSDataCal program was used for data processing (Liu et al., 2010). Most analysis spots with $^{206}Pb/^{204}Pb$ > 1000 were not corrected for common lead. Thus, analytical results with unusually high ^{204}Pb were eliminated during calculation given the influence of common lead in the inclusions. The analytical data are listed in Table 2 and graphically plotted on concordia diagrams with 1σ error. The weighted mean ages are calculated using Isoplot (Ludwig, 2003) with 2σ errors at 95% confidence.

4.3 Zircon Hf isotopic analyses

Zircon Hf isotope analysis was performed in-situ by using GeoLasPro 193 nm laser-ablation microprobe attached to Neptune multicollector ICP–MS at the Institute of Geology, Chinese Academy of Geological Sciences. Hou et al. (2007) have previously provided a comprehensive description of instrumental and data acquisition conditions. A stationary spot was used for the present analysis, with a beam diameter of 44 μm depending on the size of the ablated domains. He was used as carrier gas to transport the ablated sample from the laser -ablation cell to the ICP–MS torch via a mixing chamber filled with Ar. To correct the isobaric interferences of 176Lu and ^{176}Yb on ^{176}Hf, $^{176}Lu/^{175}Lu$=0.02658 and $^{176}Yb/^{173}Yb$=0.796218 ratios were determined (Chu et al., 2002). For instrumental mass bias correction, an exponential law was applied to normalize Yb and Hf isotope ratios to the $^{172}Yb/^{173}Yb$ ratio of 1.35274 (Chu et al., 2002) and the $^{179}Hf/^{177}Hf$ ratio of 0.7325, respectively. The mass bias behavior of Lu was assumed to follow that of Yb. Mass bias correction protocol details have been described by Hou et al (2007) in detail. Zircon GJ-1was used as the reference standard during routine analyses following the solution analysis method by Morel et al. (2006), with the weighted mean $^{176}Hf/^{177}Hf$ ratio of 0.282007±0.000007 (2σ) that was indistinguishable from the weighted mean $^{176}Hf/^{177}Hf$ ratio of 0.282000±0.000005 (2σ). The Hf model age (single-stage model age) (TDM) was calculated on the basis of a depleted-mantle source with the present-day $^{176}Hf/^{177}Hf$ ratio of 0.28325 by using the ^{176}Lu decay constant 1.865×10^{-11}a-1 (Scherer et al., 2001). The crust (two-stage) Hf model age (TDMC) was calculated on the basis of the assumption of a mean $^{176}Lu/^{177}Hf$ value of 0.015 for an average continental crust (Griffin et al., 2002).

5 Results

5.1 Major and trace elements

The major and trace element whole-rock compositions

Table 1 Major (wt%) and trace (ppm) element compositons of Yaganbuyang granitoids

Rock type	Two–mica granite						Granodiorite	
Sample No.	15CL119-2	15CL122-2	15CL123-2	15CL124-2	15CL125-2	15CL126-2	15CL125-5	15CL129-2
SiO_2	74.63	75.13	73.71	73.94	73.87	72.54	68.09	64.36
TiO_2	0.14	0.13	0.28	0.20	0.18	0.28	0.58	1.05
Al_2O_3	13.51	13.23	13.27	13.65	13.65	13.91	15.87	15.13
FeO	0.91	0.55	1.85	1.33	1.09	2.00	3.18	6.64
Fe_2O_3	0.69	0.22	0.39	0.10	0.18	0.47	0.62	1.13
MnO	0.04	0.04	0.07	0.02	0.02	0.05	0.05	0.13
MgO	0.29	0.28	0.57	0.33	0.31	0.60	0.93	1.88
CaO	1.50	0.61	1.19	1.04	1.18	1.92	2.16	2.98
Na_2O	3.76	2.46	2.33	2.74	2.46	2.89	2.79	2.79
K_2O	4.06	6.43	5.15	5.55	6.14	4.59	4.39	2.41
P_2O_5	0.07	0.13	0.13	0.08	0.07	0.04	0.18	0.19
H_2O^+	0.12	0.41	0.69	0.60	0.43	0.41	0.83	0.60
H_2O^-	0.09	0.14	0.12	0.13	0.13	0.12	0.23	0.13
Total	99.60	99.97	99.90	99.89	99.85	99.89	98.83	98.69
Ga	17.61	16.60	17.60	18.90	13.80	16.30	20.19	21.92
Rb	272.80	282.00	271.00	312.00	186.00	135.00	213.95	170.83
Sr	101.83	64.80	87.00	77.00	117.00	112.00	117.81	134.09
Y	36.89	29.90	26.70	30.20	19.90	31.50	14.23	64.04
Zr	98.66	20.60	98.90	102.00	122.00	125.00	162.22	321.92
Nb	11.86	6.67	8.66	13.00	4.24	8.64	12.83	17.83
Ba	725.58	131.00	404.00	464.00	355.00	722.00	679.04	494.74
Hf	3.23	0.77	3.14	3.11	3.74	4.18	4.89	9.97
Ta	2.52	0.60	0.83	1.45	0.32	0.66	1.15	1.05
Pb	29.15	38.00	32.90	40.90	40.00	41.40	34.01	20.01
Bi	0.31	0.21	0.23	0.61	0.07	0.08	0.34	0.05
Th	24.30	7.54	13.60	31.20	24.00	25.70	18.10	24.69
U	2.62	3.35	2.38	4.62	4.24	1.03	3.43	3.20
La	40.21	15.30	28.70	50.90	46.80	49.80	46.24	81.30
Ce	68.85	28.40	56.10	95.00	94.70	94.90	90.85	150.43
Pr	7.83	3.67	6.93	11.20	11.90	11.40	11.26	17.74
Nd	28.15	13.50	26.40	40.40	44.70	42.90	43.14	68.18
Sm	5.97	3.90	5.62	7.87	8.55	8.07	8.10	12.30
Eu	0.70	0.53	0.84	0.73	1.49	1.01	1.45	1.74
Gd	5.85	3.64	5.12	6.91	6.72	6.87	6.04	11.36
Tb	1.09	0.77	0.90	1.08	0.88	1.00	0.75	1.84
Dy	6.58	4.84	5.15	5.70	4.11	5.58	3.31	11.32
Ho	1.33	1.00	0.97	1.10	0.74	1.22	0.55	2.52
Er	3.55	2.99	2.47	2.95	2.10	3.72	1.39	7.35
Tm	0.64	0.61	0.43	0.54	0.39	0.73	0.23	1.39
Yb	3.96	4.10	2.63	3.30	2.72	5.02	1.44	9.12
Lu	0.61	0.59	0.42	0.56	0.47	0.65	0.24	1.14
REE	175.32	83.84	142.68	228.24	226.27	232.87	214.98	377.72
LREE	151.71	65.30	124.59	206.10	208.14	208.08	201.03	331.68
LREE/HREE	6.42	3.52	6.89	9.31	11.48	8.39	14.41	7.20
Eu/Eu*	0.36	0.43	0.48	0.30	0.60	0.41	0.63	0.45

of eight samples from the Yaganbuyang pluton were analyzed (Table 1). Two types of rocks (two-mica granite and granodiorite) were classified on the basis of mineral assemblage characteristics (Fig. 3a).

The two-mica granite samples exhibit SiO_2=72.54–75.13 wt%, Al_2O_3=13.23–13.91 wt%, Na_2O=2.46–3.76 wt%, K_2O=4.06–6.43 wt%, FeO^T=0.75–2.42 wt%, MgO=0.28–0.60 wt%, CaO=0.61–1.92 wt%, P_2O_5=0.04–0.13 wt%, TiO_2=0.13–0.28 wt%, Na_2O+K_2O=5.56–8.89 wt%, and K_2O/Na_2O ratios=1.08–2.61 (Table 1). These samples are distributed in the calc–alkaline to high-K calc–alkaline fields of the K_2O–SiO_2 diagram (Fig. 3b). The high K_2O contents (2.41 wt%–6.43wt %) and high K_2O/Na_2O ratios (1.08–2.61) of the samples are consistent with the geochemical characteristics of S-type granite (Chappell and White, 1974, 1992).

The chondrite-normalized REE patterns of the two-mica granite samples are shown in Fig.4a. Consistent with previous results from Li et al. (2015) and Wang et al., (2015), the samples (except for sample 15CL122-2) have total REE contents of 175.32–232.87 ppm and exhibit variable enrichment in LREE with $(La/Yb)_N$=7.28–12.34 and minor HREE fractionation with $(Gd/Yb)_N$=1.13–2.04 (Table 1). The samples showed prominently negative Eu anomalies with Eu/Eu*=0.30–0.60, indicating plagioclase fractionation (Fig. 4a, Table 1). On the primitive mantle–normalized spidergram, the samples exhibit enrichment in Rb, Th and K and significantly negative Ba, Nb, Sr, P and Ti anomalies (Fig. 4b). These characteristics are highly consistent with the characteristics of crustally derived S-

Table 2 LA–ICP–MS zircon U–Pb isotopic analyses for the samples from Yaganbuyang granitoids (Unitsfor Pb,Th and U are ppm)

Spot	Pb	Th	U	Th/U	^{207}Pb/^{206}Pb	1σ	^{207}Pb/^{235}U	1σ	^{206}Pb/^{238}U	1σ	^{207}Pb/^{206}Pb	1σ	^{207}Pb/235U	1σ	^{206}Pb/^{238}U	1σ
15CL122–3–02	229	77.2	654.6	0.1179	0.0756	0.0010	1.6520	0.0581	0.1583	0.0037	1083.3	24.5	990.3	22.3	947.6	20.9
15CL122–3–05	406	204.3	419.0	0.4875	0.0678	0.0004	1.4855	0.0185	0.1589	0.0018	864.8	25.0	924.5	7.8	950.5	10.2
15CL122–3–08	120	53.6	210.3	0.2549	0.0689	0.0013	1.5139	0.0322	0.1595	0.0029	894.4	38.9	936.0	13.1	954.1	16.0
15CL122–3–13	376	181.3	545.3	0.3324	0.0705	0.0005	1.5385	0.0246	0.1584	0.0021	942.6	11.1	945.9	10.0	948.0	12.0
15CL122–3–14	705	312.6	1108.2	0.2821	0.0686	0.0004	1.5139	0.0324	0.1603	0.0033	887.0	25.0	936.0	13.2	958.4	18.2
15CL122–3–15	486	211.8	682.4	0.3104	0.0671	0.0004	1.4844	0.0363	0.1605	0.0037	842.6	25.0	924.0	15.0	959.8	20.8
15CL122–3–21	320	146.6	627.4	0.2336	0.0705	0.0019	1.5466	0.0497	0.1592	0.0040	943.5	54.2	949.1	19.9	952.6	22.5
15CL122–3–28	256	127.2	253.6	0.5016	0.0661	0.0005	1.4683	0.0253	0.1612	0.0025	809.3	11.1	917.4	10.6	963.4	14.1
15CL122–3–30	151	68.3	256.8	0.2660	0.0667	0.0005	1.4681	0.0336	0.1597	0.0033	827.8	14.4	917.3	13.9	955.2	18.4
15CL105–3–01	89	38.3	333.8	0.1147	0.0701	0.0008	1.5885	0.0424	0.1643	0.0039	931.5	22.2	965.7	16.7	980.8	21.6
15CL105–3–02	162	60.2	872.9	0.0690	0.0700	0.0004	1.5219	0.0396	0.1577	0.0040	927.8	11.1	939.2	16.1	944.0	22.3
15CL105–3–03	112	52.5	359.9	0.1458	0.0698	0.0004	1.5903	0.0361	0.1651	0.0037	924.1	11.1	966.4	14.3	985.0	20.7
15CL105–3–04	208	97.6	728.1	0.1340	0.0703	0.0005	1.5372	0.0314	0.1585	0.0033	938.9	14.4	945.4	12.7	948.4	18.4
15CL105–3–05	119	54.5	448.3	0.1216	0.0698	0.0005	1.5624	0.0393	0.1623	0.0040	924.1	16.7	955.4	15.7	969.4	22.5
15CL105–3–06	95	43.4	291.4	0.1489	0.0699	0.0006	1.5891	0.0521	0.1649	0.0053	924.1	19.9	966.0	20.5	984.0	29.4
15CL105–3–07	131	69.1	421.0	0.1642	0.0682	0.0007	1.4813	0.0302	0.1573	0.0030	875.9	8.3	922.7	12.5	942.0	16.8
15CL105–3–08	166	102.0	286.5	0.3560	0.0690	0.0007	1.5017	0.0375	0.1578	0.0039	898.2	19.9	931.1	15.4	944.3	21.6
15CL105–3–09	338	189.4	553.6	0.3422	0.0698	0.0007	1.5235	0.0377	0.1582	0.0039	924.1	22.2	939.9	15.3	946.6	21.8
15CL105–3–10	165	86.0	324.9	0.2647	0.0711	0.0016	1.6086	0.0529	0.1641	0.0052	961.1	44.5	973.6	20.7	979.8	28.9
15CL105–3–11	411	169.3	1946.6	0.0870	0.0714	0.0007	1.5481	0.0350	0.1571	0.0036	969.4	19.9	949.7	14.1	940.7	19.9
15CL105–3–13	118	51.6	421.0	0.1227	0.0699	0.0007	1.5706	0.0379	0.1628	0.0039	927.8	19.0	958.7	15.1	972.4	21.6
15CL105–3–14	122	59.3	398.4	0.1489	0.0699	0.0007	1.5526	0.0418	0.1610	0.0042	925.0	19.9	951.5	16.7	962.5	23.4
15CL105–3–15	112	39.3	576.9	0.0682	0.0698	0.0006	1.5116	0.0308	0.1570	0.0033	924.1	16.7	935.1	12.6	940.1	18.2
15CL105–3–17	127	53.7	518.2	0.1036	0.0700	0.0006	1.5899	0.0504	0.1647	0.0050	927.8	16.7	966.3	19.9	982.9	27.8
15CL105–3–18	151	60.9	528.6	0.1151	0.0727	0.0011	1.6070	0.0718	0.1599	0.0054	1005.6	30.1	973.0	28.0	956.3	29.9
15CL105–3–19	102	44.7	391.7	0.1142	0.0698	0.0006	1.5344	0.0397	0.1593	0.0039	924.1	16.7	944.3	16.0	953.1	21.8
15CL105–3–20	137	56.5	654.5	0.0864	0.0700	0.0007	1.5217	0.0382	0.1576	0.0037	927.8	118.1	939.2	15.5	943.2	20.6
15CL105–3–23	111	45.9	487.2	0.0941	0.0700	0.0005	1.5346	0.0331	0.1590	0.0034	927.8	12.5	944.3	13.4	951.3	18.9
15CL105–3–24	156	59.4	800.9	0.0742	0.0700	0.0005	1.5181	0.0342	0.1571	0.0034	931.5	113.9	937.7	13.9	940.8	19.2
15CL105–3–25	97	46.8	314.7	0.1488	0.0701	0.0008	1.5179	0.0391	0.1571	0.0038	931.5	22.2	937.6	15.9	940.5	21.1
15CL105–3–26	110	47.9	496.0	0.0965	0.0701	0.0006	1.5126	0.0328	0.1565	0.0032	931.5	16.7	935.5	13.4	937.1	17.9
15CL105–3–29	122	49.2	534.7	0.0920	0.0700	0.0004	1.5475	0.0323	0.1602	0.0032	928.7	13.4	949.5	13.0	958.1	17.8
15CL105–3–30	147	68.9	567.3	0.1214	0.0697	0.0004	1.5166	0.0336	0.1577	0.0034	920.4	11.1	937.1	13.7	944.2	19.2
15CL123–3–03	76.0	27.4	352.1	0.0778	0.0691	0.0004	1.5091	0.0316	0.1583	0.0032	901.9	13.4	934.1	12.9	947.1	17.7
15CL123–3–04	102	37.6	457.9	0.0821	0.0689	0.0004	1.5324	0.0546	0.1613	0.0056	894.4	–2.8	943.4	22.0	963.9	31.1
15CL123–3–05	76.6	28.1	326.7	0.0860	0.0701	0.0004	1.5571	0.0351	0.1610	0.0034	931.5	108.3	953.3	14.1	962.3	19.1
15CL123–3–06	123	46.4	480.7	0.0964	0.0706	0.0004	1.5435	0.0463	0.1585	0.0047	946.3	11.1	947.9	18.6	948.3	26.0
15CL123–3–07	97	33.8	441.8	0.0766	0.0699	0.0004	1.5516	0.0374	0.1609	0.0039	925.6	14.4	951.1	15.0	961.8	21.7
15CL123–3–08	145	65.6	463.0	0.1417	0.0676	0.0005	1.4664	0.0243	0.1572	0.0029	857.4	13.4	916.6	10.2	941.4	16.5
15CL123–3–09	160	63.0	706.9	0.0892	0.0701	0.0004	1.5184	0.0300	0.1571	0.0031	931.5	108.3	937.9	12.2	940.7	17.1
15CL123–3–11	95	38.9	314.4	0.1237	0.0698	0.0005	1.5753	0.0404	0.1635	0.0040	924.1	11.1	960.5	16.0	976.4	22.3
15CL123–3–13	183	59.3	963.7	0.0615	0.0699	0.0004	1.5529	0.0300	0.1612	0.0032	924.1	11.1	951.7	12.1	963.2	17.6
15CL123–3–14	243	71.7	1305.6	0.0549	0.0709	0.0004	1.5704	0.0444	0.1605	0.0043	955.2	13.4	958.6	17.7	959.6	23.7
15CL123–3–15	110	35.4	524.8	0.0675	0.0698	0.0006	1.5418	0.0459	0.1601	0.0042	924.1	19.0	947.2	18.5	957.1	23.5
15CL123–3–16	110	47.3	320.5	0.1475	0.0700	0.0004	1.5552	0.0290	0.1612	0.0030	927.8	11.1	952.6	11.7	963.5	16.6
15CL123–3–17	114	41.4	603.1	0.0686	0.0706	0.0004	1.5628	0.0363	0.1605	0.0037	946.3	11.1	955.6	14.5	959.7	20.6
15CL123–3–18	152	58.5	622.6	0.0939	0.0690	0.0005	1.5169	0.0751	0.1593	0.0075	898.2	12.5	937.2	30.4	953.1	41.9
15CL123–3–20	136	49.7	630.6	0.0788	0.0695	0.0005	1.4962	0.0387	0.1562	0.0039	922.2	11.1	928.8	15.9	935.5	22.0
15CL123–3–21	119	43.6	504.9	0.0864	0.0700	0.0005	1.5859	0.0521	0.1642	0.0052	929.3	113.9	964.7	20.6	980.1	29.1
15CL123–3–22	123	44.1	443.1	0.0994	0.0712	0.0007	1.5740	0.0392	0.1603	0.0037	964.8	4.2	960.0	15.6	958.3	20.4
15CL123–3–23	160	55.4	765.6	0.0724	0.0699	0.0004	1.5532	0.0552	0.1611	0.0057	927.8	14.4	951.8	22.0	962.7	31.7
15CL123–3–24	126	56.7	353.7	0.1604	0.0701	0.0004	1.5237	0.0341	0.1576	0.0034	931.5	108.3	940.0	13.9	943.2	19.1
15CL123–3–26	169	57.7	771.4	0.0748	0.0699	0.0005	1.5210	0.0284	0.1578	0.0030	924.1	13.4	938.9	11.6	944.8	16.7
15CL123–3–28	108	36.2	499.9	0.0724	0.0697	0.0006	1.5506	0.0677	0.1613	0.0071	920.4	8.3	950.7	27.0	964.1	39.4
15CL123–3–29	234	39.8	1319.5	0.0302	0.0723	0.0006	1.5922	0.0583	0.1595	0.0049	994.4	33.8	967.2	22.9	953.8	27.5
15CL123–3–30	987	547.1	683.3	0.8007	0.0695	0.0005	1.5240	0.0268	0.1590	0.0026	922.2	13.4	940.1	10.9	951.1	14.5
15CL129–3–01	318	175.1	520.5	0.3365	0.0702	0.0007	1.5840	0.0386	0.1636	0.0037	1000.0	19.0	964.0	15.3	976.9	20.6
15CL129–3–02	128	67.1	261.6	0.2566	0.0712	0.0007	1.5574	0.0204	0.1587	0.0020	964.8	5.1	953.4	8.3	949.3	11.2
15CL129–3–03	174	91.9	449.9	0.2042	0.0697	0.0006	1.4804	0.0185	0.1540	0.0015	920.4	16.7	922.4	7.8	923.2	8.6
15CL129–3–04	158	87.8	288.6	0.3044	0.0699	0.0006	1.4924	0.0257	0.1548	0.0024	925.0	16.7	927.3	10.6	928.0	13.4
15CL129–3–05	153	90.4	222.0	0.4074	0.0697	0.0006	1.4773	0.0302	0.1536	0.0029	920.4	16.7	921.1	12.5	921.1	16.1
15CL129–3–06	120	66.5	224.1	0.2968	0.0698	0.0006	1.4889	0.0328	0.1546	0.0033	924.1	19.0	925.9	13.5	927.0	18.5
15CL129–3–09	137	77.2	208.3	0.3708	0.0700	0.0007	1.5388	0.0359	0.1593	0.0035	929.3	113.9	946.0	14.5	953.0	19.8
15CL129–3–10	112	55.5	293.0	0.1893	0.0699	0.0006	1.5627	0.0454	0.1620	0.0046	927.8	16.7	955.5	18.1	967.8	25.4
15CL129–3–11	124	70.9	225.4	0.3147	0.0697	0.0006	1.4901	0.0262	0.1550	0.0026	920.4	2.8	926.3	10.8	929.1	14.6
15CL129–3–12	147	74.6	373.2	0.1999	0.0692	0.0006	1.4778	0.0398	0.1548	0.0037	905.6	18.1	921.3	16.4	927.7	20.6
15CL129–3–15	126	72.8	219.0	0.3323	0.0700	0.0005	1.5335	0.0309	0.1589	0.0032	927.8	13.4	943.9	12.5	950.5	18.0
15CL129–3–17	78	42.4	149.7	0.2832	0.0706	0.0017	1.5631	0.0579	0.1604	0.0038	946.3	46.8	955.7	23.0	958.9	21.3
15CL129–3–20	523	303.4	940.2	0.3227	0.0702	0.0005	1.5286	0.0378	0.1580	0.0038	933.0	16.7	942.0	15.3	945.4	21.3
15CL129–3–21	366	195.7	888.5	0.2202	0.0702	0.0005	1.5169	0.0284	0.1566	0.0028	1000.0	12.5	937.2	11.6	937.7	15.6
15CL129–3–22	94	52.0	216.1	0.2408	0.0701	0.0006	1.5552	0.0343	0.1609	0.0036	931.5	16.7	952.6	13.8	961.9	19.9
15CL129–3–23	220	111.5	425.7	0.2618	0.0703	0.0005	1.5639	0.0380	0.1614	0.0038	936.1	16.7	956.0	15.2	964.4	21.4
15CL129–3–24	132	75.5	256.6	0.2944	0.0703	0.0005	1.4963	0.0234	0.1544	0.0022	936.7	16.7	928.9	9.7	925.3	12.1
15CL129–3–25	135	75.7	239.5	0.3162	0.0701	0.0004	1.5701	0.0349	0.1623	0.0036	932.4	13.4	958.5	13.9	969.6	19.9
15CL129–3–30	107	62.8	189.5	0.3316	0.0703	0.0005	1.5273	0.0312	0.1577	0.0031	1000.0	13.4	941.4	12.7	943.7	17.6

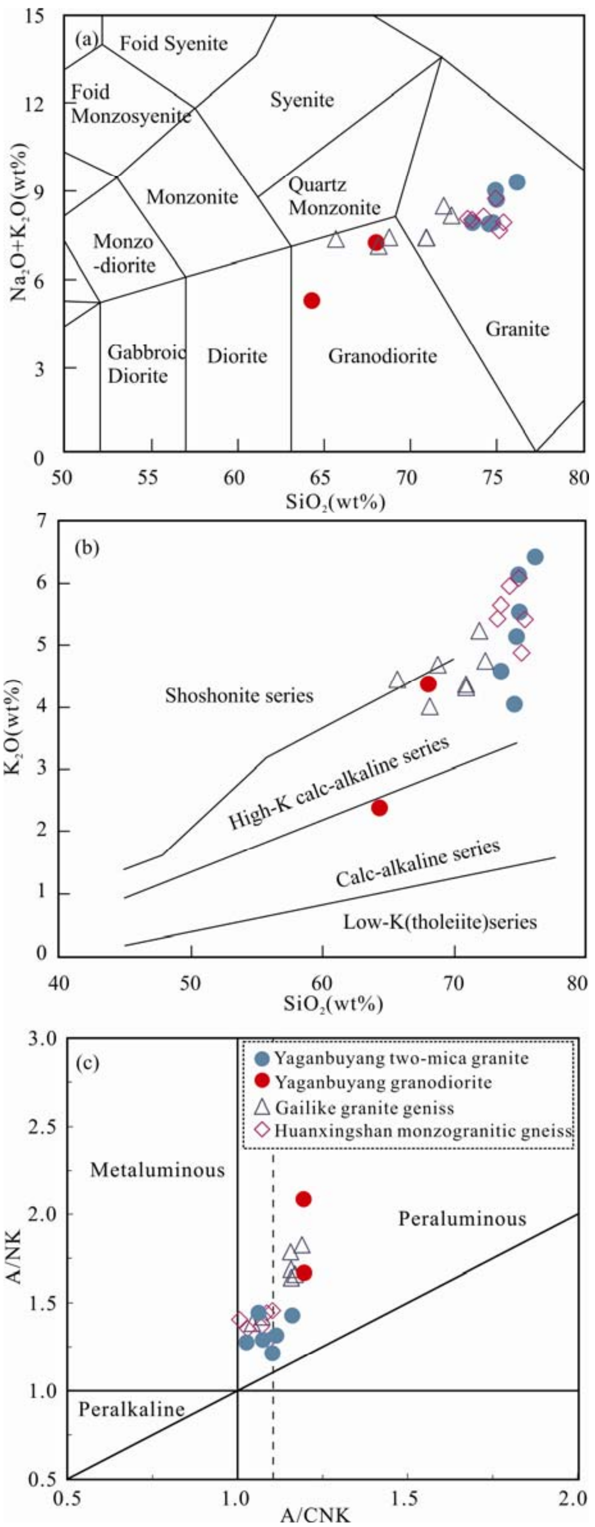

Fig. 3. (a), TAS diagram (b), SiO_2 vs. K_2O diagram (c), A/CNK vs. A/NK diagram; (a, after Middlemost, 1994; b, after Martin et al., 2005; c, after Maniar and Piccoli, 1989; Gailike and Huanxingshan data from Li et al., 2015; Wang et al, 2015).

type magmas (Gao et al., 1998). The REE and trace-element patterns of the samples are similar to those of Neoproterozoic (880–926Ma) peraluminous granitoids in the Altyn Tagh Orogen belt (Li et al., 2015; Wang et al., 2015). Compared with those of other samples, the geochemical characteristics of sample 15CL122-2 are more anomalous. Sample 15CL122-2 exhibits lower contents of FeO^T+MgO+TiO_2=1.18 wt% and higher ratios of CaO/Na_2O (0.25) and Al_2O_3/TiO_2 (107.7) than other samples. The total REE contents of 83.84 ppm, $(La/Yb)_N$=2.67 and $(Gd/Yb)_N$=0.73 indicate prominently negative Zr, Hf anomalies with Zr/Hf ratios of 26.75 and correspond to the characteristics of high–differentiation granite (Breiter et al., 2014; Wu et al.,2017).

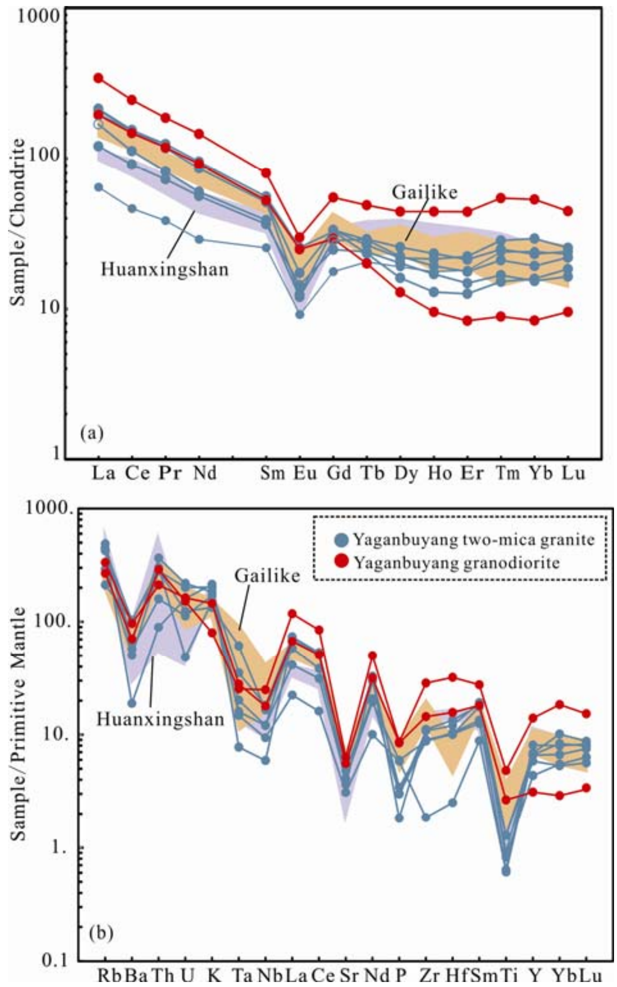

Fig. 4. Chondrite-normalized REE patterns (a) and primitive mantle-normalized multiple trace element (b) diagrams of the Yaganbuyang pluton (Data for chondrite and primitive mantle -normalizing values are from Sun and McDonough (1989).

The major elemental contents of granodiorite samples are SiO_2=64.36–68.09 wt%, Al_2O_3=15.13–15.87 wt%, Na_2O=2.79 wt%, K_2O=2.41–4.39 wt%, FeO^T=3.74–7.65 wt%, MgO=0.93–1.88 wt%, CaO=2.16–2.98 wt%, P_2O_5=0.18–0.19 wt%, TiO_2=0.58–1.05 wt%, Na_2O+K_2O =5.20–7.18 wt%, and K_2O/Na_2O=0.86–1.57 (Table 1). These samples are distributed in the subalkaline granodiorite fields on the TAS diagram (Fig. 3a) and are strongly peraluminous with A/CNK ratios of 1.20 (Fig. 3c). The chondrite-normalized REE patterns of the granodiorite are shown in Fig. 4a. The total REEs of the samples are in the range of 214.98–377.72 ppm. The samples exhibit variable enrichment in LREE with $(La/Yb)_N$ = 6.39–23.09, minor HREE fractionation with $(Gd/Yb)_N$ = 1.03–3.48 (Table 1), and prominently negative Eu anomalies with Eu/Eu^*=0.45–0.63 indicative of plagioclase fractionation (Fig. 4a, Table 1). On the primitive mantle–normalized spidergram, the samples exhibit enrichment in Rb, Th, and K and significantly negative Ba, Nb, Sr, P and Ti anomalies (Fig. 4b).

5.2 Zircon U–Pb ages

The zircons of four samples from the Yaganbuyang granitoids are subhedral–euhedral and long prismatic. They have lengths of 50–200 μm and length/width ratios of 1.5:1–3:1. Cathodoluminescence images of the Yaganbuyang granitoids (Fig. 5) show that most zircon grains exhibit oscillatory zoning that is indicative of igneous origin. Moreover, some zircons have dark edges, which resulted from later metamorphism. Zircon U–Th–Pb isotopic data are listed in Table 2. The cathodoluminescence images of representative zircons are shown on in Fig. 5.

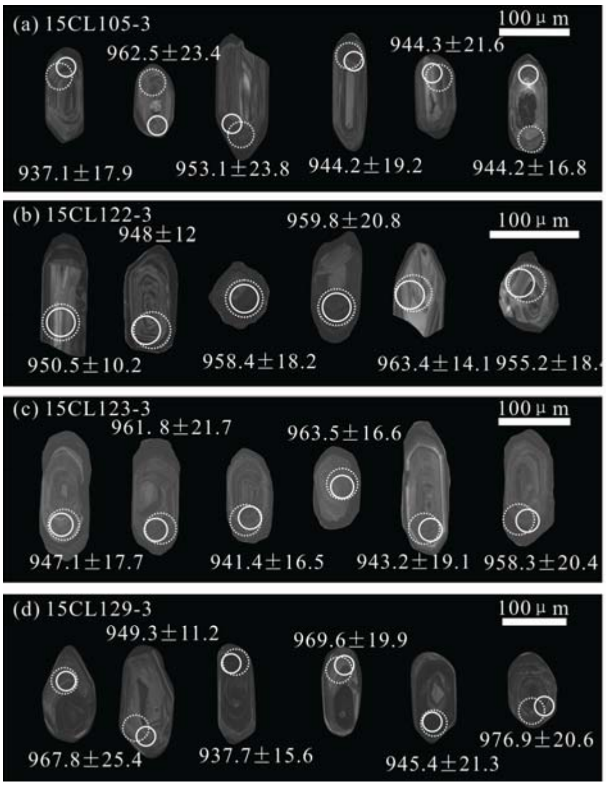

Fig. 5. Cathodoluminescence images of representative zircons from the Yaganbuyang pluton. Solid and dashed circles indicate the spots subjected to LA–ICP–MS U–Pb and Hf analyses, respectively.

Sample 15CL105-3 (two-mica granite). These zircons have Th contents of 38.3–189.4 ppm, U contents of 286.5–1946.6 ppm, and Th/U ratios of 0.07–0.36 (Table 2). Among the 27 analysis spots, 24 are concordant and yielded a weighted mean $^{206}Pb/^{238}U$ age of 953.3±8.4 Ma (MSWD=0.54) (Fig. 6a), which is interpreted as the crystallization age of the two-mica granite. Spots #16, #21, and #27 are inherited/xenocrystic cores and zircons with $^{206}Pb/^{238}U$ ages of 1698±29.5, 1166.8±30.1, and 1066±30.7 Ma, respectively.

Sample 15CL122-3 (two-mica granite). These zircons have Th contents of 53.6–312.6 ppm, U contents of 210.3–1108.2 ppm, and Th/U ratios of 0.12–0.50 (Table 2). Nine of the 20 analysis spots are concordant and yield a weighted mean $^{206}Pb/^{238}U$ age of 954±10 Ma (MSWD=0.13) (Fig. 6b), which is interpreted as the crystallization age of the two-mica granite. The remaining spots are inherited/xenocrystic cores and zircons and provided $^{206}Pb/^{238}U$ ages of 1013–1692 Ma.

Sample 15CL123-3 (garnet-bearing two-mica granite). These zircons have Th contents of 27.4–547.1 ppm, U contents of 86.1–1319.5 ppm, and Th/U ratios of 0.03–1.03 (Table 2). Among the 26 analysis spots, 23 are concordant and yield a weighted mean $^{206}Pb/^{238}U$ age of 954.1±8.5 Ma (MSWD=0.27) (Fig. 6c), which is interpreted as the crystallization age of the garnet-bearing two-mica granite. Spots #1, #10, and #19 are inherited/xenocrystic cores and zircons and provided $^{206}Pb/^{238}U$ ages of 1009.1±23.6, 1010.3±20.7, and 1601±28.2 Ma, respectively.

Sample 15CL129-3 (granodiorite). These zircons have Th contents of 41.5–303.4 ppm, U contents of 149.7–940.2 ppm, and Th/U ratios of 0.20–0.41 (Table 2). Nineteen of the 20 analysis spots are concordant and provided a weighted mean $^{206}Pb/^{238}U$ age of 939±7.1 Ma (MSWD=1.13) (Fig. 6d), which is interpreted as the crystallization age of the granodiorite. The remaining spots are inherited cores and provided $^{206}Pb/^{238}U$ ages of 1292.2±31 Ma.

5.3 Zircon Hf isotopes

The zircons used for U–Pb dating were subjected to in-situ zircon Hf analyses. The analytical results are listed in Table 3. The plots of $\varepsilon_{Hf}(t)$ values versus zircon U–Pb ages are shown in Fig. 7. A total of 65 spots were analyzed. The results showed that all $^{176}Lu/^{177}Hf$ ratios are less than 0.002, indicating that radiogenic Hf isotope accumulation is low after zircon formation. The ratios of $^{176}Lu/^{177}Hf$ can be used to represent the Hf isotopic composition of zircons during crystallization.

The initial $^{176}Hf/^{177}Hf$ ratio of sample 15CL105-3 is in the range of 0.281948–0.282341, which corresponds to the

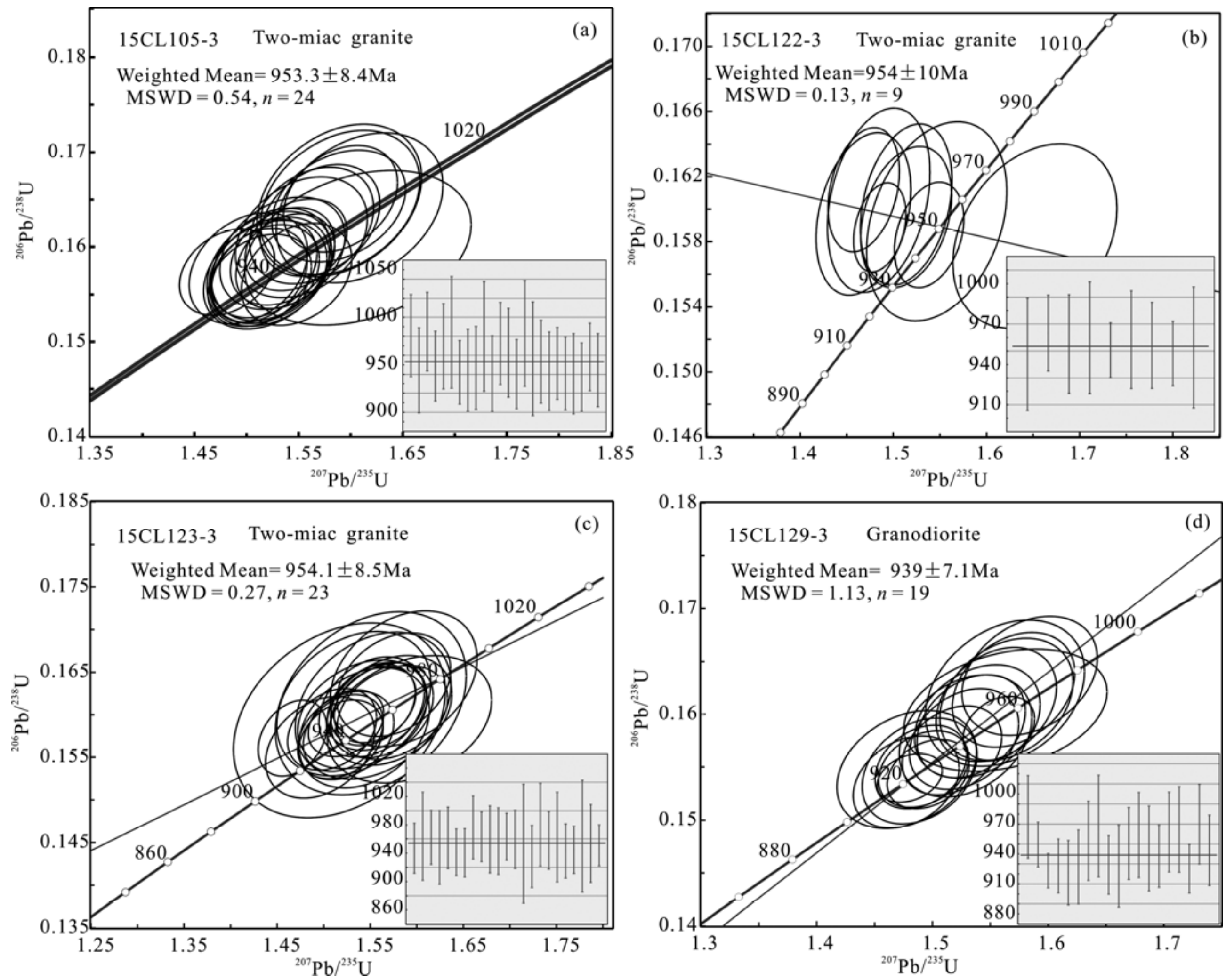

Fig. 6. Concordia diagrams of zircons U–Pb data for samples from the Yaganbuyang pluton.

$\varepsilon_{Hf}(t)$ values of −8.64 to +5.19 and the Hf model ages (T_{DM2}) of 1.70–2.35 Ga. The initial $^{176}Hf/^{177}Hf$ ratio of sample 15CL122-3 is in the range of 0.282129–0.282263 and corresponds to the $\varepsilon_{Hf}(t)$ value of −1.65 to +2.91 and Hf model ages (T_{DM2}) of 1.62–1.92 Ga. The initial $^{176}Hf/^{177}Hf$ ratio of sample 15CL123-3 is in the range of 0.282111–0.282224 and corresponds to the $\varepsilon_{Hf}(t)$ value of −2.85 to +1.19 and the Hf model ages (T_{DM2}) of 1.74–1.99 Ga. The initial $^{176}Hf/^{177}Hf$ ratio of sample 15CL129-3 is in the range of 0.282098–0.282360 and corresponds to the $\varepsilon_{Hf}(t)$ value of −3.93 to +5.30 and the Hf model ages (T_{DM2}) of 1.59–2.05Ga (Fig. 7, Table 3). These $\varepsilon_{Hf}(t)$ values reflect that ancient crust is the predominant contributor to the magma source, which also has been influenced by juvenile crust.

6 Discussion

6.1 Petrogenesis

Geochemistry data show that Yaganbuyang granitoids belong to peraluminous calc–alkaline to high-K calc–alkaline granite with high A/CNK ratios. In general, peraluminous granitoids form in the subductional and regional extensional environment or as a response to the thickening and anatexis of the orogenic belt crust (Barbarin., 1996; Collins., 1998; Douce and Harris., 1998; Sylvester., 1998; Douce., 1999; Healy et al., 2004; Chen et al., 2014). Experimental petrology has shown that peraluminous granitic silicate melts can be produced by the partial melting of various sources under certain temperature and pressure conditions (Rapp and Watson., 1991, 1995; Winther and Newton., 1996). The compositional variation of the plutons depends on the components of the initially molten substances, melting temperature, pressure, and the difference in the initial water content (Hansen et al., 2002). Generally, acidic peraluminous granitoids are derived from the partial melting of clastic sedimentary materials, whereas high-K aluminum-rich granitoids are derived from pelite–greywacke sedimentary materials (Johannes and Holtz.,

Table 3 LA–ICP–MS zircon Hf isotopic analyses for the samples from Yaganbuyang granitoids

Sample	Age	$^{176}Yb/^{177}Hf$	2σ	$^{176}Lu/^{177}Hf$	2σ	$^{176}Hf/^{177}Hf$	2σ	$^{176}Hf/^{177}Hf(T)$	$\varepsilon_{Hf}(t)$	t_{DM}	t_{DM2}	$f_{Lu/Hf}$
15CL105–3–01	953.3	0.049816	0.000833	0.001190	0.000016	0.281953	0.000017	0.281932	–8.639	1835	2355	–0.96
15CL105–3–02	953.3	0.026043	0.001367	0.000575	0.000031	0.282239	0.000014	0.282229	1.880	1413	1696	–0.98
15CL105–3–03	953.3	0.039330	0.000418	0.000946	0.000008	0.282153	0.000014	0.282136	–1.421	1547	1903	–0.97
15CL105–3–04	953.3	0.048257	0.002070	0.001118	0.000042	0.282181	0.000013	0.282161	–0.522	1514	1847	–0.97
15CL105–3–05	953.3	0.059499	0.000434	0.001415	0.000007	0.282076	0.000014	0.282051	–4.421	1673	2091	–0.96
15CL105–3–06	953.3	0.069499	0.000279	0.001645	0.000007	0.282182	0.000014	0.282152	–0.837	1535	1866	–0.95
15CL105–3–08	953.3	0.038711	0.001633	0.000913	0.000033	0.282175	0.000015	0.282159	–0.597	1514	1851	–0.97
15CL105–3–09	953.3	0.030940	0.001424	0.000724	0.000030	0.282171	0.000013	0.282158	–0.647	1513	1854	–0.98
15CL105–3–10	953.3	0.030136	0.000642	0.000736	0.000022	0.282219	0.000014	0.282206	1.061	1447	1747	–0.98
15CL105–3–11	953.3	0.110700	0.003872	0.002703	0.000090	0.282268	0.000016	0.282219	1.536	1454	1717	–0.92
15CL105–3–13	953.3	0.031968	0.001806	0.001029	0.000083	0.282341	0.000021	0.282322	5.190	1288	1487	–0.97
15CL105–3–14	953.3	0.033686	0.002224	0.000794	0.000048	0.282219	0.000012	0.282205	1.027	1449	1749	–0.98
15CL105–3–15	953.3	0.025703	0.001749	0.000712	0.000062	0.282213	0.000015	0.282200	0.853	1454	1760	–0.98
15CL105–3–18	953.3	0.026162	0.000606	0.000627	0.000015	0.281948	0.000016	0.281937	–8.476	1815	2345	–0.98
15CL105–3–19	953.3	0.043663	0.001267	0.001028	0.000027	0.282190	0.000014	0.282171	–0.167	1499	1824	–0.97
15CL105–3–20	953.3	0.025802	0.000537	0.000633	0.000020	0.282241	0.000016	0.282230	1.912	1412	1694	–0.98
15CL105–3–23	953.3	0.017726	0.000342	0.000402	0.000008	0.282175	0.000014	0.282167	–0.295	1495	1832	–0.99
15CL105–3–25	953.3	0.042219	0.002054	0.000997	0.000049	0.282163	0.000014	0.282145	–1.105	1535	1883	–0.97
15CL105–3–26	953.3	0.017185	0.000175	0.000396	0.000005	0.282144	0.000014	0.282137	–1.384	1537	1901	–0.99
15CL105–3–29	953.3	0.013512	0.000444	0.000303	0.000012	0.282120	0.000014	0.282115	–2.165	1565	1950	–0.99
15CL105–3–30	953.3	0.045598	0.002893	0.001083	0.000071	0.282188	0.000016	0.282169	–0.253	1503	1830	–0.97
15CL122–3–05	954	0.032164	0.002723	0.000906	0.000069	0.282166	0.000015	0.282150	–0.916	1527	1872	–0.97
15CL122–3–13	954	0.045526	0.000585	0.001300	0.000017	0.282152	0.000016	0.282129	–1.651	1562	1918	–0.96
15CL122–3–14	954	0.046163	0.000321	0.001357	0.000009	0.282279	0.000018	0.282254	2.804	1386	1638	–0.96
15CL122–3–15	954	0.062076	0.001733	0.001839	0.000038	0.282296	0.000021	0.282263	3.096	1380	1620	–0.94
15CL122–3–28	954	0.029920	0.001219	0.000819	0.000032	0.282206	0.000019	0.282192	0.572	1467	1778	–0.98
15CL122–3–30	954	0.027843	0.002298	0.000799	0.000066	0.282245	0.000021	0.282230	1.943	1413	1692	–0.98
15CL123–3–03	954.1	0.019153	0.000486	0.000466	0.000009	0.282133	0.000016	0.282125	–1.787	1554	1927	–0.99
15CL123–3–04	954.1	0.037083	0.000479	0.000916	0.000017	0.282145	0.000016	0.282129	–1.657	1556	1918	–0.97
15CL123–3–05	954.1	0.042280	0.000816	0.001206	0.000031	0.282123	0.000019	0.282101	–2.633	1599	1980	–0.96
15CL123–3–06	954.1	0.042664	0.000504	0.001088	0.000018	0.282115	0.000019	0.282095	–2.844	1606	1993	–0.97
15CL123–3–07	954.1	0.012900	0.000147	0.000303	0.000002	0.282165	0.000014	0.282159	–0.564	1504	1850	–0.99
15CL123–3–08	954.1	0.032008	0.000241	0.000805	0.000005	0.282154	0.000017	0.282140	–1.253	1539	1893	–0.98
15CL123–3–11	954.1	0.035679	0.001319	0.000897	0.000030	0.282169	0.000018	0.282153	–0.779	1521	1863	–0.97
15CL123–3–13	954.1	0.024060	0.000347	0.000575	0.000009	0.282137	0.000019	0.282126	–1.733	1554	1923	–0.98
15CL123–3–14	954.1	0.046968	0.000922	0.001069	0.000011	0.282149	0.000015	0.282130	–1.614	1557	1916	–0.97
15CL123–3–17	954.1	0.017175	0.000763	0.000424	0.000018	0.282216	0.000015	0.282209	1.187	1438	1740	–0.99
15CL123–3–18	954.1	0.037853	0.000844	0.000968	0.000015	0.282152	0.000016	0.282135	–1.445	1549	1905	–0.97
15CL123–3–20	954.1	0.023754	0.000731	0.000636	0.000023	0.282188	0.000016	0.282176	0.037	1486	1812	–0.98
15CL123–3–21	954.1	0.026925	0.000404	0.000705	0.000012	0.282198	0.000017	0.282185	0.345	1475	1793	–0.98
15CL123–3–22	954.1	0.039840	0.000685	0.001015	0.000015	0.282183	0.000016	0.282165	–0.379	1507	1838	–0.97
15CL123–3–23	954.1	0.031140	0.000454	0.000794	0.000010	0.282155	0.000015	0.282141	–1.221	1537	1891	–0.98
15CL123–3–24	954.1	0.047710	0.001257	0.001230	0.000025	0.282174	0.000017	0.282152	–0.820	1528	1866	–0.96
15CL123–3–26	954.1	0.037085	0.000570	0.000871	0.000018	0.282111	0.000016	0.282095	–2.851	1602	1993	–0.97
15CL123–3–28	954.1	0.027111	0.000282	0.000676	0.000009	0.282170	0.000016	0.282158	–0.624	1512	1854	–0.98
15CL123–3–29	954.1	0.052536	0.001429	0.001393	0.000029	0.282171	0.000014	0.282146	–1.037	1539	1879	–0.96
15CL123–3–30	954.1	0.046886	0.000936	0.001225	0.000020	0.282224	0.000020	0.282202	0.956	1458	1754	–0.96
15CL129–3–01	939	0.042244	0.000435	0.001155	0.000023	0.282281	0.000021	0.282261	2.691	1375	1634	–0.97
15CL129–3–02	939	0.052069	0.001091	0.001237	0.000027	0.282254	0.000019	0.282232	1.674	1417	1698	–0.96
15CL129–3–03	939	0.063632	0.000379	0.001560	0.000014	0.282248	0.000017	0.282221	1.277	1437	1723	–0.95
15CL129–3–04	939	0.068046	0.000903	0.001665	0.000022	0.282207	0.000017	0.282177	–0.266	1500	1820	–0.95
15CL129–3–05	939	0.046328	0.000883	0.001145	0.000016	0.282249	0.000018	0.282228	1.544	1421	1706	–0.97
15CL129–3–06	939	0.061876	0.001020	0.001532	0.000023	0.282290	0.000018	0.282263	2.783	1376	1628	–0.95
15CL129–3–09	939	0.051818	0.000613	0.001338	0.000029	0.282275	0.000018	0.282251	2.343	1391	1656	–0.96
15CL129–3–11	939	0.058730	0.000435	0.001484	0.000007	0.282236	0.000018	0.282209	0.867	1452	1748	–0.96
15CL129–3–12	939	0.056917	0.001251	0.001491	0.000024	0.282296	0.000018	0.282270	3.005	1367	1614	–0.96
15CL129–3–15	939	0.056690	0.000583	0.001371	0.000009	0.282212	0.000017	0.282188	0.095	1481	1797	–0.96
15CL129–3–17	939	0.065161	0.000801	0.001415	0.000005	0.282238	0.000018	0.282213	0.995	1446	1740	–0.96
15CL129–3–20	939	0.087542	0.001143	0.002023	0.000034	0.282248	0.000019	0.282212	0.974	1455	1742	–0.94
15CL129–3–21	939	0.072342	0.000843	0.001788	0.000021	0.282256	0.000018	0.282225	1.408	1435	1714	–0.95
15CL129–3–22	939	0.060976	0.001640	0.001353	0.000030	0.282098	0.000018	0.282074	–3.926	1640	2049	–0.96
15CL129–3–23	939	0.057634	0.000839	0.001429	0.000038	0.282360	0.000018	0.282334	5.296	1275	1469	–0.96
15CL129–3–24	939	0.061213	0.000566	0.001406	0.000007	0.282304	0.000018	0.282280	3.355	1352	1592	–0.96
15CL129–3–25	939	0.047970	0.001490	0.001085	0.000028	0.282301	0.000018	0.282282	3.435	1345	1587	–0.97
15CL129–3–30	939	0.066995	0.001397	0.001551	0.000024	0.282279	0.000020	0.282252	2.369	1393	1654	–0.95

1996; Sisson et al., 2004). The value of $Mg^{\#}$ is an important index for judging the source of the magmatic melt. $Mg^{\#}$ values of less than 40 indicate that the magmatic melt is formed by the partial melting of the crust, whereas high $Mg^{\#}$ values indicate mantle-source substances (Rapp et al., 1995). The $Mg^{\#}$ values of the Yaganbuyang granitoids are in the range of 25.6–40.0 with an average of 31.1, indicating that the granitoids are

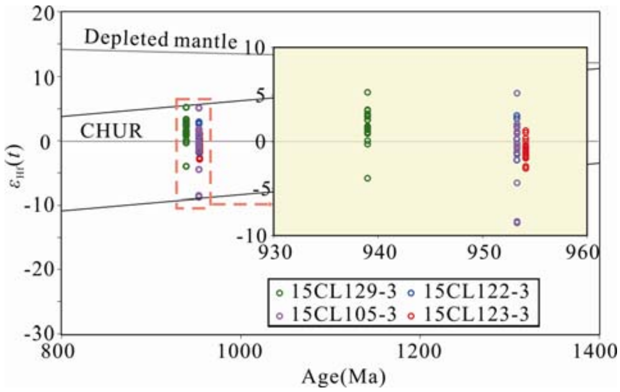

Fig.7. Hf isotopic compositions of zircons from granitoids from the Yaganbuyang pluton.

mainly derived from partial crustal melting.

The two-mica granite presented high SiO_2, K_2O, and NaO content and high A/CNK values. P_2O_5 and SiO_2 contents are positively correlated (Fig. 8a). The two-mica granite also show negative Eu anomalies in their chondrite-normalized REE patterns and negative Ba, Ta, Nb, Sr, P, and Ti anomalies in their mantle–normalized trace-element patterns. In the C/MF–A/MF diagram (Fig. 9a), all two-mica granite samples (except 15CL122-2) fall into the greywacke-derived melt area, whereas the granodiorite samples are close to the basalt-derived melt area. In the Al_2O_3+FeO^T+MgO+TiO_2 versus Al_2O_3/ FeO^T+MgO+ TiO_2) diagram (Fig. 9b), the two-mica granite samples also fall in the greywacke-derived melt area, whereas granodiorite falls into the basalt-derived melt area (Douce et al., 1999). CaO/Na_2O ratios vary in the range of 0.25–1.07 with an average of 0.56, and almost all values (except for 15CL122-2) exceed 0.3 (Fig. 9c). FeO^T/MgO ratios fall in the range of 2.67–4.30, Al_2O_3/TiO_2 ratios fall in the range of 47.4–101.7 with an average of 68.6, and K_2O/Na_2O ratios fall in the range of 1.59–2.61, indicating a greywacke sedimentary origin in the continental crust (Sylvester et al., 1998). The Zr/Hf ratios (26.75–32.80) are slightly lower than that in the upper crust (−37) (Gao et al., 1998). In the Rb/Sr versus Rb/Ba diagram (Fig. 9d), all samples fall into the greywacke-derived area. The variable $\varepsilon_{Hf}(t)$ values of −8.64 to +5.19 indicate isotope disequilibrium in magma. Moreover, such variability indicates that the source rocks are mainly from the Paleoproterozoic–Proterozoic crust and are affected by the juvenile crust during evolution (Fig. 7). All these features indicate that the granitoids are mainly derived from sedimentary components. The geochemical characteristics of sample 15CL122-2 are significantly different from those of other samples. Specifically, this sample has higher SiO_2 (75.13%), K_2O (6.43%), and DI index (94.1) and lower TiO_2 (0.13), FeO^T (0.75), MgO (0.28) and CaO/Na_2O (0.25) than other samples. In the Zr+Nb+Ce+Y versus K_2O+Na_2O/CaO diagram (Fig. 8b), sample 15CL122-2 falls into the high-fractionation granite area, with negative anomalies of Zr and Hf with a Zr/Hf ratio of 26, indicating that it is the product of highly fractionated magma in the late stage of magmatic activity.

Granodiorite is enriched in Al_2O_3 FeO^T, MgO, and TiO_2 and has an A/CNK ratio of 1.2. Fig. 8a shows the different trends of P_2O_5, versus SiO_2 contents presented by two-mica granites. The chondrite-normalized REE patterns of the two-mica granite exhibit negative Eu anomalies, and its mantle–normalized trace element patterns exhibit negative Ba, Ta, Nb, Sr, P and Ti anomalies (Fig. 4). In the C/MF versus AMF diagram, the samples are close to the area of the basalt-derived melt. In the Al_2O_3+FeO^T+ MgO+TiO_2 versus Al_2O_3/(FeO^T+MgO+TiO_2) diagram (Fig. 9b) the samples fall into the area of basalt-derived

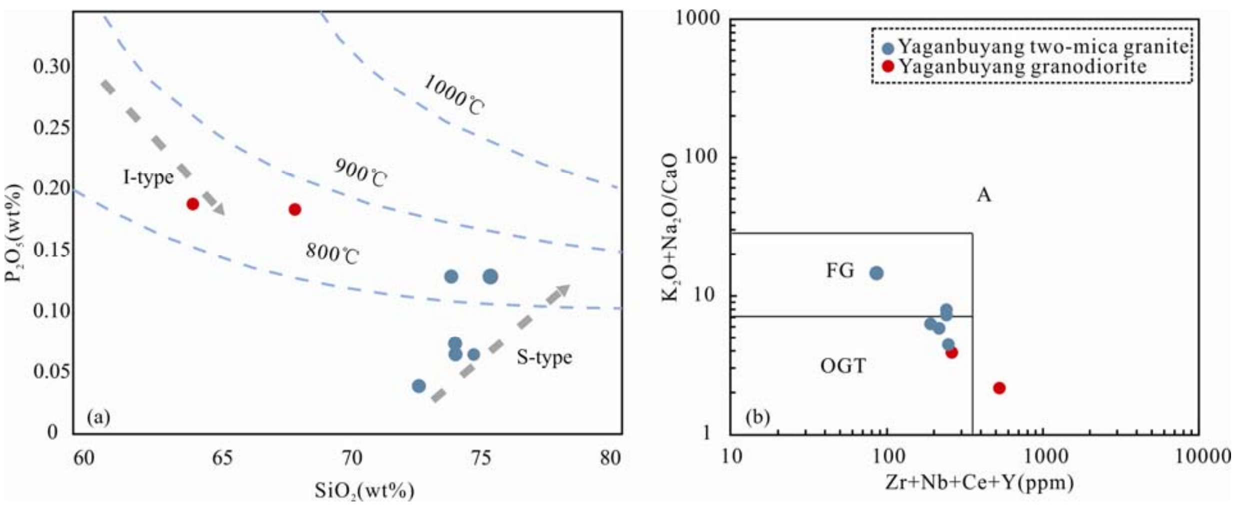

Fig. 8. (a) Whole-rock SiO_2 vs. P_2O_5 diagram of granitoids in the Yaganbuyang area; (b) Zr+Nb+Ce+Y–Na_2O+K_2O/CaO diagram (a after Xin et al., 2017; b after Whalen et al., 1987)
FG-Fractionated granites; OGT- Unfractionated I-, S-, and M-type granites.

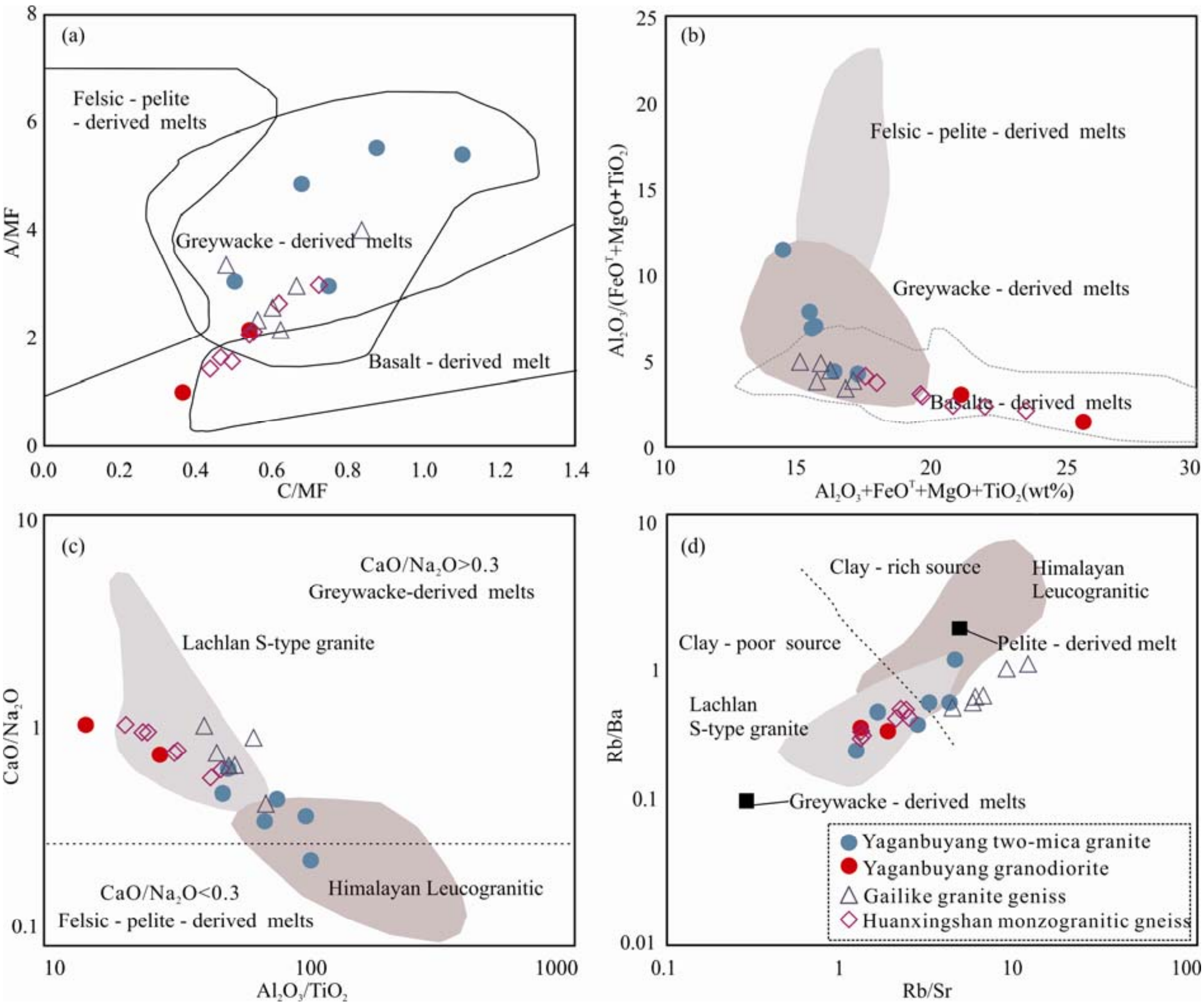

Fig. 9. Geochemical diagrams of granitoids in the Yaganbuyang area.
(a), C/MF vs. A/MF (after Alther et al.,2000); (b), Al_2O_3+FeO^T+MgO+TiO_2 vs. Al_2O_3/(FeO^T+MgO+TiO_2) (after Douce,1999); (c), Al_2O_3 /TiO_2 vs. CaO/Na_2O; and (d), Rb/Sr vs. Rb/Ba (after Sylvester,1998). Data sources: Himalayan leucogranites (after Searle and Fryer, 1986; Inger and Harris, 1993; Ayres and Harris, 1997) and Lachlan S–type granites (after Chappell and Simpson, 1984; Healy et al., 2004).

melt (Douce et al., 1999). The Nb/Ta ratios (11.11–17.06) are similar to the crust (Nb/Ta=12–13) (Barth et al., 2000). The Zr/Hf ratios (32.28–33.19) are slightly lower than the upper crust (~37) (Gao et al., 1998). The variable $\varepsilon_{Hf}(t)$ values of −3.92 to +5.29 imply that Hf isotope disequilibrium exists in magma (Fig. 7). These features indicate that the source rocks have the characteristics of lower crustal basalt rocks.

6.2 Neoproterozoic magmatism

The magmatic zircons from the Yaganbuyang have similar ages of 939–954 Ma, which are highly consistent with the previously reported magmatic ages for the Altyn Tagh Orogen belt and represent a Neoproterozoic magmatic event. Two-mica granite formed earlier than granodiorite and shows different source characteristics. Thus, the upwelling of mantle materials may have caused the partial melting of crustal materials. The two-mica granite is derived from the melting of crustal sediments, and granodiorite is derived from the melting of lower mafic crust. The Gailike pluton in the adjacent area has a U–Pb age of 886.5±5 Ma and may have a mafic crustal origin (Li et al., 2015). The Huanxingshan pluton in the western segment of the Altyn Tagh Orogen belt has a zircon U–Pb age of 928±7.7 Ma and is a S-type granite formed by melting of crustal sedimentary materials (Wang et al., 2015). Granitoids of the Altyn Complex have a zircon U–Pb age of 920–940 Ma (Zhang et al., 2011). All these granitoids demonstrate the existence of an early Neoproterozoic magmatic arc in the South Altyn Tagh (Wang et al., 2013). In addition, many Early Paleozoic granites and eclogites are exposed in the South Altyn Tagh Orogen belt, suggesting that these Neoproterozoic granitic rocks may be affected by Paleozoic tectonic events (Wang et al., 2006; 2013; Yu et al., 2013a).

Early Neoproterozoic granite and granitic gneiss with similar formation ages are well preserved in the surrounding areas. For example, granitic gneiss with an age of 907–1002 Ma is present in the North Qaidam UHMP belt of the Qaidam basin (Lin et al., 2006; Song et al., 2012). Granite and mafic rocks with ages of 910–942 and 905–919 Ma, respectively, are present in the Qilian Massif (Guo et al., 1999; Gehrels et al., 2003; Wan et al., 2003; Tung et al., 2007, 2012). Granite emplacements in the North Qinling Orogen have ages of 900–980 Ma (Pei et al., 2007; Lu et al., 2005; Wang et al., 2005). The syn-orogenic granite in East Kunlun, aged 904–940 Ma, indicates the occurrence of tectono–thermal activity within East Kunlun during the Mesoproterozoic to early Neoproterozoic (Meng et al., 2011). Neoproterozoic metamorphic events have been reported in North Qaidam but not in Altyn Tagh Orogen (Zhang et al., 2008; Yu et al., 2013a). Nevertheless, the similar magmatism and metamorphism ages in these regions indicate that the widespread magmatism that occurred in the Central Orogenic belt during early Neoproterozoic is related to the convergence and breakup of the Rodinia supercontinent.

6.3 Tectonic implications

The Rodinia supercontinent was constructed when the Grenville orogeny (ca. 1300–900 Ma) formed belts that welded together a series of continental blocks and microcontinental fragments (Hoffman,1991; Mabi et al., 2018). Rodinia assembled through worldwide orogenic events that occurred between 1300 and 900 Ma, with all continental blocks known to exist at that time likely being involved. By ca. 900 Ma, all major known continental blocks had aggregated to form the Rodinia supercontinent (Li et al., 2008).

Numerous Neoproterozoic magmatic and metamorphic events in the Altyn–Qilian–Qaidam have been previously reported (Guo et al.,1999; Wan et al., 2003,2006; Wang et al., 2006, 2013; Xu et al,2007; Lu et al., 2002, 2006, 2008; Tung et al., 2007, 2012; Zhang et al.,2008, 2011;Song et al., 2012; Yu et al., 2010, 2011, 2013a), and the Neoproterozoic granitoids in the northern margin of the region are thought to originate from intermediate–basic volcanic rocks in active continental margin settings (Song et al., 2012; Wang et al., 2013; Yu et al., 2013a). During the early Neoproterozoic, the northern margins of the

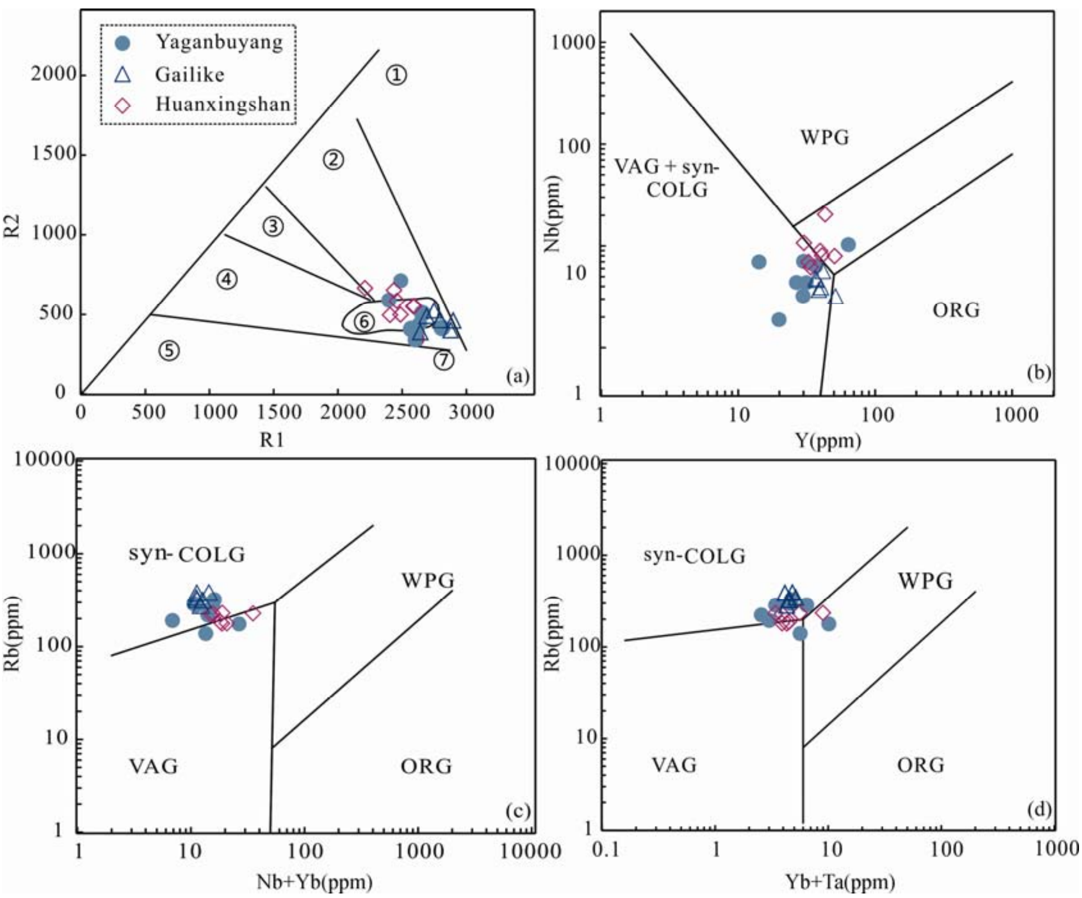

Fig.10. (a) R_1–R_2 discrimination diagrams (a, after Bachlor et al., 1985); (b), Nb–Y diagram, (c), Rb–(Nb+Yb) diagram and (d), Rb–(Yb+Ta) diagram (b, c, d, after Pearce et al.,1984)

①mantle differentiation products; ②before plate collision; ③post collision uplift; ④late orogenic stage; ⑤non orogenic; ⑥syn collision; ⑦post orogenic.

Altyn–Qilian–Qaidam and Tarim plates might have combined to form an integrated block that was temporarily connected to the northern part of South China Craton or to the west of Rodinia at the later stage of the Grenville orogeny (950–900 Ma) (Zhang et al., 2011;Yu et al., 2013a). Several ancient blocks, including the Tarim block, middle Altyn Tagh microcontinent, and Qaidam block existed in the Altyn Tagh tectonic belt during the Middle Proterozoic (1.3–1.8 Ga). The convergence of these blocks during the Neoproterozoic led to the melting of sediments in the continental margin and the formation of S-type granites (Qin et al., 2006, 2008). Recent studies have shown that most Neoproterozoic granitic rocks in the Altyn Tagh area present syn-collisional characteristics, and Neoproterozoic magmatic events may be related to the convergence of the Rodinia supercontinent (Wang et al., 2006, 2013; Yu et al., 2013a; Li et al., 2015).

Similar to continental-collision granite, Yaganbuyang granitoids have Nb and Ta contents of 6.67–13 ppm and 0.32–1.45 ppm, respectively, and a Nb/Ta=8.9–13.2 (Pearce et al., 1984). The R_1–R_2 diagram shows that the samples are related to a syn–collisional setting (Fig. 9e). In the Nb–Y, Rb versus (Nb+Yb) and Rb versus (Yb+Ta) diagrams (Fig. 9e), almost all samples fall into the syn-collision area. All the characteristics exhibited above indicate that the Yaganbuyang granitoids formed in a continental-collision environment.

The Altyn Tagh provides records of the formation of syn-collision granitoids during the early Neoproterozoic (900–940 Ma). The formation of granitoids is a response to the formation of the Rodinia supercontinent and is a large-scale collisional orogenic event that occurred simultaneously with the Grenville orogeny (Liu et al., 2009b; Yu et al., 2013a; Wang et al., 2013). This large-scale collision orogenic event eventually consolidated the metamorphic basement of Tarim (Lu et al., 2008).

7 Conclusion

New data from this study enabled us to draw the following conclusions:

(1) Yaganbuyang granitoids consist mainly of two-mica granite and granodiorite. Geochemical data suggested that the Yaganbuyang granitoids are mainly composed of peraluminous calc–alkaline to high-K calc–alkaline granite with magmatic zircon U–Pb ages of 939+7.1 and ~954 Ma, respectively.

(2) Zircon Hf isotopic data showed that the $\varepsilon_{\mathrm{Hf}}(t)$ values of the two-mica granite are −3.93 to +5.30 with Hf model ages (T_{DM2}) of 1.59–2.05 Ga. The $\varepsilon_{\mathrm{Hf}}(t)$ values of the granodiorite are −8.64 to +5.19 with Hf model ages (T_{DM2}) of 1.62–2.35 Ga. These data indicated that the magma is predominantly derived from ancient crust, with contributions from juvenile crust.

(3) The granitoids formed in a collisional orogenic belt that may have been induced by the convergence of the Rodinia supercontinent during the Neoproterozoic.

Acknowledgements

This work was financially supported by the Projects of the China Geological Survey (Grant No. 12120115027001, 121201102000150005-06) and Natural Science Foundation of China (Grant No.41272079, 41302266).

Manuscript received Dec. 5, 2017
accepted May 8, 2018
edited by Fei Hongcai

References

Agyei–Dwarko, N.Y., Augland, L.E., and Andresen, A., 2012. The Heggmovatn supracrustals, North Norway-a late Mesoproterozoic to early Neoproterozoic (1050–930 Ma) terrane of Laurentian origin in the Scandinavian Caledonides. *Precambrian Research*, 212–213: 245–262.

Alther, R., Holl, A., Hegner, E., Langer, C., and Kreuzer, H., 2000. High-potassium, calc-alkaline I-type plutonism in the European Variscides: Northern Vosges (France) and northern Schwarzwald (Germany). *Lithos*, 50(1–3): 51–73.

Ayres, M., and Harris, N., 1997. REE fractionation and Nd–isotope disequilibrium during crustal anatexis: Constraints from Himalayan leucogranites. *Chemical Geology*, 139(1–4): 249–269.

Barbarin, B., 1996. Genesis of the two main types of peraluminous granitoids. *Geology*, 24(4): 295–298

Barth, M.G., Mcdonough, W.F., and Rudnick, R.L., 2000. Tracking the budget of Nb and Ta in the continental crust. *Chemical Geology*, 165(3–4): 197–213.

Batchelor, R.A., and Bowden, P., 1985. Petrogenetic interpretation of granitoid rock series using multicationic parameters. *Chemical Geology*, 48(1): 43–55.

Bonin, B., 2007. A-type granites and related rocks: evolution of a concept, problems and prospects. *Lithos*, 97: 1–29.

Breiter, K., Lamarão, C.N., Borges, R.M.K., and Dall' Agnol, R., 2014. Chemical characteristics of zircon from A–type ranites and comparison to zirconof S-type granites. *Lithos*, 192–195 (2): 208–225

Brown, M., 1993. P-T-t evolution of orogenic belts and the causes of regional metamorphism. *Journal of the Geological Society*, 150: 227–241.

Brown, M., 2001. Orogeny, migmatites and leucogranites: a review. *Journal of Earth System Science*, 110: 313–336.

Cao, Y.T., Liu, L., Wang, C., Chen, D.L., and Zhang, A.D., 2009. P-T path of early Paleozoic pelitic high-pressure granulite from Danshuiquan area in Altyn Tagh. *Acta Petrologica Sinica*, 25: 2260–2270 (in Chinese with English abstract)

Chappell, B.W., and White, A.J.R., 1974. Two contrasting granite types. *Pacific Geology*, 8: 173–174.

Chappell, B.W., and White, A.J.R, 1992. I- and S-type granites in the Lachlan fold belt. *Transactions of the Royal Society of Edinburgh Earth Sciences*, 83(1–2): 1–26.

Chappell, B.W., and White, A.J.R., 2001. Two contrasting granite types: 25 years later. *Journal of the Geological Society of Australia*, 48(4): 489–499.

Chappell, B.W., and Simpson, P.R., 1984. Source rocks of I- and S-type granites in the Lachlan fold belt, southeastern Australia [and discussion]. *Philosophical Transactions of the Royal Society of London*. Series A, Mathematical and Physical Sciences, 310(1514): 693–707.

Che, Z.C., Liu, L., Liu, H.F., and Luo, J.H., 1995. Discovery and occurrence of high pressure metapelitic rocks from Altun Mountain areas, Xinjiang Autonomous Region. *Chinese Science Bulletin*, 40 (14): 1298–1300 (in Chinese).

Chen, N.S., Li, X.Y., Wang, X.Y., Chen, Q., Wang, Q.Y., and Wan, Y.S., 2006. Zircon SHRIMP U-Pb age of Neoproterozoic metagranite in the North Kunlun unit on the southern margin of the Qaidam block in China. *Geological Bulletin of China*, 25(11): 1311–1314 (in chinese with English abstract).

Chen, Y.X., Song, S.G., Niu, Y.L., and Wei, C.J., 2014. Melting of continental crust during subduction initiation: A case study from the Chaidanuo peraluminous granitein the North Qilian suture zone. *Geochimica et Cosmochimica Acta*, 132: 311–336.

Chu, N.C., Taylor, R.N., Chavagnac, V., Nesbitt, R.W., Boella, R.M., Milton, J.A., German, C.R., Bayon, G., and Burton, K., 2002. Hf isotope ratio analysis using multicollector inductively coupled plasma mass spectrometry: an evaluation of isobaric interference corrections. *Journal of Analytical Atomic Spectrometry*, 17: 1567–1574.

Collins, W.J., 1998. Evolution of petrogenetic models for Lachlan fold belt granitoids: Implications for crustal architecture and tectonic models. *Australian Journal of Earth Science*, 45(4): 483–500.

Cui, J.W., 2011. Ductile shearing age of the south altun fault and its tectonic implications. *Acta Petrologica Sinica*, 27(11): 3422–3434.

Douce, A.E.P., and Harris, N., 1998. Experimental constraints on Himalayan anatexis. *Journal of Petrology*, 39(4): 689–710.

Douce, A.E.P., 1999. What do experiments tell us about the relative contributions of crust and mantle to the origin of granitic magmas? In: Castro, A., Fernandez, C., and Vigneresse, J.L. (eds.), *Understanding Granites: Integrating New and Classical Techniques*. Geological Society, London, Special Publications, 168: 55–75.

Gao, S., Luo, T.C., Zhang, B.R., Zhang, H.F., Han, Y.W., Zhao, Z.D., and Hu, Y.K., 1998. Chemical composition of the continental crust as revealed by studies in East China. *Geochimicaet Cosmochimica Acta*, 62(11): 1959–1975

Gehrels, G.E., Yin, A., and Wang, X., 2003. Magmatic history of the northeastern Tibetan Plateau. *Journal of Geophysical Research*, 108: 1–14.

Griffin, W.L., Wang, X., Jackson, S.E., Pearson, N.J., O'Reilly, S.R., Xu, X.S., and Zhou, X.M., 2002. Zircon chemistry and magma mixing, SE China: In-situ analysis of Hf isotopes, Tonglu and Pingtan igneous complexes. *Lithos*, 61(3–4): 237–269.

Guo, J.J., Zhao, F.Q., and Li, H.K., 1999. Jinningian collisional granite belt in the eastern sector of the Central Qilian massif and its implication. *Acta Geoscientia Sinica*, 20(1): 10–15 (in Chinese with English abstract)

Hansen, J., Skjerlie, K.P., Pedersen, R.B., and De La Rosa, J., 2002. Crustal melting in the lower parts of island arcs: An example from the Bremanger granitoid Complex, west Norwegian Caledonides. *Contribution of Mineral Petrology*, 143(3): 316–335.

Healy, B., Collins, W.J., and Richards, S.W., 2004. A hybrid origin for Lachlan S-type granites: The Murrumbidgee Batholith example. *Lithos*, 78(1–2): 197–216.

Hoffman, P.F., 1991. Did the breakout of Laurentia turn Gondwanaland inside-out? *Science*, 252: 891–901.

Hou, K.J., Li, Y.H., and Tian, Y.Y., 2009. In situ U–Pb zircon dating using laser ablation-multi ion counting-ICP-MS. *Mineral Deposits*, 28(4): 481–492 (in Chinese with English abstract).

Hou, K.J., Li, Y.H., Zou, T.R., Qu, X.M., Shi, Y.R., and Xie, G.Q., 2007. Laser ablation-MC-ICP-MS technique for Hf isotope microanalysis of zircon and its geological applications. *Acta Petrologica Sinica*, 23(10): 2595–2604 (in Chinese with English abstract).

Inger, S., and Harris, N., 1993. Geochemical constraints on leucogranite magmatism in the Langtang Valley, Nepal Himalaya. *Journal of Petrology*, 34(2): 345–368.

Jackson, S.E., Pearson, N.J., Griffin, W.L., and Belousova, E.A., 2004. The application of laser ablation-inductively coupled plasma-mass spectrometry to in situ U-Pb zircon geochronology. *Chemical Geology*, 211(1): 47–69.

Johannes, W., and Holtz, F., 1996. *Petrogenesis and experimental petrology of granitic rocks*. Berlin Heibelderg: Springer-Verlag.

Li, Q., Zeng, Z.C., Chen, N., Zhao, J., Zhang, R.Y., Yi, P.F., Gao, H.F., and Bi, J.Z., 2015. Zircon U-Pb ages, geochemical characteristics and tectonic implications of Neoproterozoic gailike gneiss in the South Altyn Tagh. *Geoscience*, 6: 1271–1283 (in Chinese with English abstract).

Li, Z.X., Bogdanova, S.V., Collins, A.S., Davidson, a., De Waele, B., Ernst, R.E., Fitzsimons, I.C.W., Fuck, R.a., Gladkochub, D.P and Jacobs, J., 2008. Assembly, configuration, and break-up history of Rodinia: a synthesis. *Precambrian Research*, 160: 179–210.

Lin, C.L., Sun, Y., Chen, D.L., Diwu, C.R., 2006. Geochemistry and zircon LA-ICP-MS dating of Iqe River granitic gneiss, northern margin of Qaidam Basin. *Geochimica*, 35: 489–505.

Liu, L., Che, Z.C., Luo, J.H., Wang, Y., and Gao, J.Z., 1996. Recognition and implication of eclogite in the western Altun Mountains, Xinjiang. *Chinese Science Bulletin*, 41(14): 1458–1488 (in Chinese).

Liu, L., Che, Z.C., Wang, Y., Luo, J.H., and Chen, D.L., 1999. The petrological character and geotectonic setting of high pressure metamorphic rock belts in Altun Mountains. *Acta Petrologica Sinica*, 15(1): 57–64 (in Chinese with English abstract).

Liu, L., Wang, C., Cao, Y.T., Chen, D.L., Kang, L., Yang, W.Q., and Zhu, X.H., 2012. Geochronology of multi-stage metamorphic events: Constraints on episodic zircon growth from the UHP eclogite in the South Altyn, NW China. *Lithos*, 136–139: 10–26.

Liu, L., Wang, C., Chen, D.L., Zhang, A.D., and Liou, J.G., 2009a. Petrology and geochronology of HP-UHP rocks from the South Altyn Tagh, northwestern China. *Journal of Asian*

Earth Sciences, 35(3–4): 232–244.

Liu, L., Zhang, A.D., Chen, D.L., Yang, J.X., Luo, J.H., and Wang, C., 2007a. Implications based on LA-ICP-MS zircon U -Pb ages of eclogite and its country rock from Jianggalesayi Area, Altyn Tagh, China. *Earth Science Frontiers*, 14: 98–107.

Liu, L., Zhang, J.F., Green, H.W.II., Jin, Z.M., and Bozhilov, K.N., 2007b, Evidence of former stishovite in metamorphosed sediments, implying subduction to > 350 km. *Earth and Planetary Science Letters*. 263(3–4): 180–191.

Liu, Y.S., Gao, S., Hu, Z.C., Gao, C.G., Zong, K.Q., and Wang, D.B., 2010. Continental and oceanic crust recycling-induced melt-peridotite interactions in the Trans-North China Orogen: U-Pb dating, Hf isotopes and trace elements in zircons from mantle xenoliths. *Journal of Petrology*, 51(1–2): 537–571.

Liu, Y.S., Yu, H.F., Xin, H.T., Lu, S.N., Xiu, Q.Y., and Li, Q., 2009b. Tectonic units division and Precambrian significant geological events in Altyn Tagh Mountain, China. *Geological Bulletin of China*, 28 (10): 1430–1438 (in Chinese with English abstract).

Liu, C.H., Wu, C.L., Gao, Y.H., Lei, M., and Qin, H.P., 2016. Age, composition, and tectonic significance of palaeozoic granites in the Altyn orogenic belt, China. *International Geology Review*, 58(2): 131–154.

Lu, S.N., Li, H., Zhang, C., and Niu, G., 2008. Geological and geochronological evidence for the Precambrian evolution of the Tarim craton and surrounding continental fragments. *Precambrian Research*, 160(1–2): 94–107.

Lu, S.N., 1998. A review of advance in the research on the Neoproterozoic Rodinia supercontinent. *Geological Review*, 44(5): 489–495 (in Chinese with English abstract).

Lu, S.N., 2002. Discussion on the new subdivision of the Neoproterozoic in China. *Journal of Geological Review* 48: 242–248 (in Chinese with English abstract).

Lu, S.N., Chen, Z.H., Li, H.K., and Hao, G.J., 2005. Two magmatic belts of the Neoproterozoic in the Qinling orogenic belt. *Acta Geologica Sinica*, 79: 165–173 (in Chinese with English abstract).

Lu, S.N., Yu, H.F., and Li, H.K., 2006. *Research on Precambrian major problems in China*. Beijing: Geological Publishing Press, 1–206 (in Chinese with English abstract).

Ludwig, K.R., 2003. *User's manual for Isoplot3.0: A geochronological toolkit for Microsoft Excel*. Berkeley: Berkeley Geochronology Center.

Mabi, A., Yang, Z.X., Zhang, M.C., Wen, D.K., Li, Y.L., and Liu, X.Y., 2018. Two types of granites in the western Yangtze Block and their implications for regional tectonic evolution: Constraints from geochemistry and isotopic data. *Acta Geologica Sinica* (English Edition), 92(1): 89–105.

Maniar, P.D., and Piccoli, P.M., 1989. Tectonic discrimination of granitoids. *Geological Society of America Bulletin*, 101(5): 635–643.

Martin, H., Smiithies, R.H., Rapp, R., Moyen, J.F., and Champion, D., 2005. An overview of adakite, tonalite-trondhjemite-granodiorite (TTG), and sanukitoid: Relationships and some implications for crustal evolution. *Lithos*, 79(1–2): 1–24.

Mei, H.L., Li, H.M., Lu, S.N., Yu, H.F., Zuo, Y.C., and Li, C., 1999. The age and origin of the Liuyuan granitoid, northwestern Gansu. *Acta Petrologicaet Mineralogica*, 18 (1): 14–17 (in Chinese with English abstract).

Meng, F.C., Cui, M., and Wu, X., 2011. East Kunlun early Neoproterozoic granite and its tectonic implication. In: *National Symposium on Petrology and Geodynamics Abstracts*. 253.

Middlemost, E.A.K., 1994. Naming materials in the magma/ igneous rock system. *Earth Science Reviews*, 37(3–4):193–227.

Milani, L., Lehmann, J., Naydenov, K.V., Saalmann, K., Kinnaird, J.A., Daly, J.S., Frei, D., and Sanz, A.L.G., 2015. A –type magmatism in a syn-collisional setting: The case of the Pan-African hook batholith in Central Zambia. *Lithos*, 216–217: 48–72.

Nasdala, L., Hofmeister, W., Norberg, N., Martinson, J.M., Corfu, F., Dörr, W., Kamo, S.L., Kennedy, A.K., Kronz, A., Reiners, P.W., Frei, D., Kosler, J., Wan, Y.S., Götze, J., Häger, T., Alfred Kröner, A., and Valley, J.W., 2008. Zircon M257–a homogeneous natural reference material for the ion microprobe U-Pb analysis of zircon. *Geostandards & Geoanalytical Research*, 32(3): 247–265.

Pearce, J.A., Harris, N.B.W., and Tindle, A.G., 1984. Trace element discrimination diagrams for the tectonic interpretation of granitic rocks. *Petrology*, 54(4): 956–983.

Pei, X.Z., Ding, S.P., Zhang, G.W., Liu, H.B., Li, Z.C., Li, W.Y., Liu, Z.Q and Meng, Y., 2007. Zircons LA-ICP-M S U-Pb dating of Neoproterozoic granitoid gneisses in the north margin of West Qinling and geological implication. *Acta Geologica Sinica*, 81: 772–786 (in Chinese with English abstract).

Qin, X.F., Li, J., Lu, J.P., Xu, H., Hu, G.A., Zhou, F.S., and Li, Q., 2006. Tectonic evolution of the western segment of the Altyn Tagh collisional orogen, northwest China. *Geological Bulletin of China*, 25: 104–112 (in Chinese with English abstract).

Qin, X.F., Xia, B., Li, C.Q., Li, J., Lu, J.P., Xu, H., Zhou, F.S., Hu, G.E., and Li, Q., 2008. Geochemical characteristics and tectonic setting of Precambrian granitic gneiss in the western segment of Altyn Tagh Tectonic belt. *Geoscience*, 22(1): 34–44.

Rapp, R.P., and Watson, E.B., 1995. Dehydration melting of metabasalt at 8–32 kbar: Implications for continental growth and crust-mantle recycle. *Journal of Petrology*, 36(4): 891–931.

Rapp, R.P., Watson, E.B., and Miller, C.F., 1991. Partial melting of amphibolite/eclogite and origin of Archean trondhjemites and tonalities. *Precambrian Research*, 51(4): 1–25.

Scherer, E., Munker, C., and Mezger, K., 2001. Calibration of the Luteitium-Hafnium clock. *Science*, 293(5530): 683–687.

Searle, M.P., and Fryer, B.J., 1986. Garnet, tourmaline and muscovite-bearing leucogranites, gneisses and migmatites of the Higher Himalayas from Zanskar, Kulu, Lahoul and Kashmir. *Geological Society of London Special Publications*, 19(1): 185–201.

Sisson, T.W., Ratajeski, K., Hankins, W.B., and Glazner, A.F., 2004. Voluminous granitic magmas from ommon basaltic sources. *Contributions to Mineralogy and Petrology*, 148(6): 635–661.

Sláma, J., Košler, J., Daniel, J.C., Crowley, J.L., Gerdes, A., Hanchar, J.M., Horstwood, M.S.A., Morris, G.A., Nasdala, L., Norberg, N., Schaltegger, U., Schoene, B., Tubrett, M.N., and Whitehouse, M.J., 2008. Plešovice zircon-A new natural reference material for U-Pb and Hf isotopic microanalysis.

Chemical Geology, 249(1–2): 1–35.

Song, S.G., Su, L., Li, X.H., Niu, Y.L., and Zhang, L.F., 2012. Grenvile-age orogenesis in the Qaidam-Qilian block: the link between South China and Tarim. *Precambrian Research*, 220–221(8): 9–22.

Song, S.G., Wang, M.J., Wang, C., and Niu, Y.L., 2015. Magmatism during continental collision, subduction, exhumation and mountain collapse in collisional orogenic belts and continental net growth: a perspective. *Science China: Earth Sciences*, 58: 1284–1304.

Sun, S.S., McDonough, W.F., 1989. Chemical and isotopic systematics of ocean basalts: implication for mantle composition and processes. In: Saunders, A.D., and Norry, M.J. (eds.), *Magmatism in Ocean Basins*, vol. 42. Geological Society Special Publication: 313–345.

Sylvester, P.J., 1998. Post-collisional strongly peraluminous granites. *Lithos*, 45(1–4): 29–44.

Tung, K.A., Yang, H.J., Yang, H.Y., Liu, D.Y., Zhang, J.X., Wan, Y.S., and Tseng, C.Y., 2007. SHRIMP U-Pb geochronology of the zircons from the Precambrian basement of the Qilian Block and its geological significances. *Chinese Science Bulletin*, 52: 2687–2701.

Tung, K.A., Yang, H.Y., Liu, D.Y., Zhang, J.X., Yang, H.J., Shau, Y.H and Tseng, C.Y., 2012.The amphibolite-facies metamorphosed mafic rocks from the Maxianshan area, Qilian block, NW China: a record of early Neoproterozoic arc magmatism. *Journal of Asian Earth Sciences* 46: 177–189.

Wan, Y.S., Zhang, J.X., Yang, J.S., and Xu, Z.Q., 2006. Geochemistry of high-grade metamorphic rocks of the North Qaidam Mountains and their geological significance. *Journal of Asian Earth Sciences*, 28: 174–184.

Wan, Y.S., Xu, Z.Q., Yang, J.S and Zhang, J.X., 2003. The Precambrian high-grade basement of the Qilian terrane and neighboring areas: its ages and compositions. *Acta Geoscientia Sinica*, 24: 319–324.

Wang, C., Liu, L., Che, Z.C., Chen, D.L., Zhang, A.D., and Luo, J.H., 2006. U–Pb Geochronology and tectonic setting of the granitic gneiss in Jianggaleisayi eclogite belt, the southern edge of Altyn Tagh. *Geological Journal of China Universities*, 12 (1): 74–82 (in Chinese with English abstract).

Wang, C., Liu, L., Yang, W.Q., Zhu, X.H., Cao, Y.T., Kang, L., Chen, S.F., Li, R.S., and He, S.P., 2013. Provenance and ages of the Altyn complex in Altyn Tagh: Implications for the Early Neoproterozoic evolution of northwestern China. *Precambrian Research*, 230: 193–208.

Wang, C., Liu, H., Deng, J.H., Liu, X.F., Zhao, F.F., Wang, C., and Tian, X., 2018. Isotope geochronologic and geochemical constraints on the magmatic associations of the collisional orogenic zone in the West Kunlun Orogen, China, *Acta Geologica Sinica* (English Edition), 92(2): 482–498.

Wang, L.S., Zhang, W., Duan, X.X., Long, X.P., Ma, Z.P., Song, Z.B., and Sun, J.M., 2015. Isotopic age and genesis of the monzogranitic gneiss at the Huanxingshan in middle Altyn Tagh. *Acta Petrologica Sinica*, 31(1): 119–132 (in Chinese with English abstract).

Wang, C., Liu, L., Chen, D.L., Cao, Y.T., 2011. Petrology, geochemistry, geochronology and metamorphic volution of garnet peridotites from South Altyn Tagh UHP terrane, NW China: Records related to crustal slab subduction and exhumation history. In: Dobrzhinetskaya, L., Faryad, W., Wallis, S., and Cuthbert, S. (eds.), *Ultrahigh Pressure Metamorphism: 25 Years after the Discovery of Metamorphic Coesite and Diamond*. Elsevier, 541–576.

Wang, T., Zhang, Z.Q., Wang, X.X., Wang, Y.B., and Zhang, C.L., 2005. Neoproterozoic collisional deformation in the core of the qinling orogen and its age: constrained by zircon SHRIMP dating of strongly deformed syn-collisional granites and weakly deformed granitic veins. *Acta Geologica Sinica*, 79(2): 220–231 (in Chinese with English abstract).

Whalen, J.B., Currie, K.L., and Chappell, B.W., 1987. A-type granites: geochemical characteristics, discrimination and petrogenesis. *Contributions to Mineralogy and Petrology*, 95: 407–419.

Whitney, D.L., and Evans, B.W., 2010. Abbreviations for names of rock-forming minerals. *American Mineralogist*, 95(1): 185–187.

Winther, K.T., and Newton, R.C., 1996. Experimental melting of hydrous low-K tholeiite: Evidence on the origin of Archean cratons. *Bulletin of the Geological Society of Denmark*, 39: 213–228.

Wu, C.L., Gao, Y.H., Lei, M., Qin, H.P., Liu, C.H., Li, M.Z., Frost, B.R., and Wooden, J.L., 2014. South Altyn Tagh Mangai granitoids SHRIMP U-Pb zircon dating, Lu-Hf isotope geochemistry and petrogenesis. *Acta Petrologica Sinica*, 30(8): 2297–2323 (in Chinese with English abstract).

Wu, C.L., Lei, M., Wu, D., Zhang, X., Chen, H.J., and Li, T.X., 2016. Zircon U-Pb dating of Paleozoic granites from South Altun and response of the magmatic activity to the tectonic evolution of the Altun orogenic belt. *Acta Geologica Sinica*, 90(9): 2276–2315 (in Chinese with English abstract).

Wu, C.L., Yang, J.S., Robinson, P.T., Wooden, J.L., Mazdab, F.K., Gao, Y.H., Wu, S.P., and Chen, Q.L., 2009, Geochemistry, age and tectonic significance of granitic rocks in north Altun, northwest China. *Lithos*, 113(3–4):423–436.

Wu, F.Y., Liu, X.C., Ji, W.Q., Wang, J.M., and Yang, L., 2017. Highly fractionated granites: Recognition and research. *Science China Earth Sciences*, 60: 1201–1219 (in Chinese).

Xin, Y.J., Li, J.H., Dong, S.W., Zhang, Y.Q., Wang, W.B., and Sun, H.S., 2017. Neoproterozoic post-collisional extension of the central Jiangnan orogen: geochemical, geochronological, and Lu-Hf isotopic constraints from the ca. 820–800 Ma magmatic rocks. *Precambrian Research*, 294: 91–110.

Xu, Z.Q., Yang, J.S., Zhang, J.X., Jiang, M., Li, H.B., and Cui, J.W., 1999. A comparison between the tectonic units on the two sides of the Altun sinistral strike fault and the mechanism of lithospheric shearing. *Acta Geologica Sinica*, 73(3): 193–205 (in Chinese with English abstract).

Xu, W.C., Zhang, H.F., and Liu, X.M., 2007. U-Pb zircon dating constraints on formation time of 483 Qilian high-grade metamorphic rock and its tectonic implications. *Chinese Science Bulletin*, 52: 531–538.

Yu, H.F., Lu, S.N., Liu, Y.S., Xiu, Q.Y., and Li, Q., 2002. Composition of the Altyn Tagh formation-complex and its tectonic signification. *Geological Bulletin of China*, 21(12): 834–840 (in Chinese with English abstract)

Yu, S.Y., and Zhang, J.X., 2010. Provenance and age of gneisses in the Dulan area, North Qaidam UHP metamorphic belt: Evidence from zircon U-Pb geochronology, REE and Hf isotopic analyses. *Acta Petrologica Sinica*, 26(7): 2083–2098 (in Chinese with English abstract).

Yu, S.Y., Zhang, J.X., and Gong, J.H., 2011. Zr-in-rutile thermometry in HP/UHT granulite in the bashiwake area of the South Altun and its geological implications. *Earth science frontiers*, 18(2): 140–150 (in Chinese with English abstract).

Yu, S.Y., Zhang, J.X., Li, H.K., Hou, K.J., Mattinson, C.G., and Gong, J.H., 2013b. Geochemistry, zircon U-Pb geochronology and Lu-Hf isotopic composition of eclogites and their host gneisses in the Dulan area, North Qaidam UHP terrane: New evidence for deep continental subduction. *Gondwana Research*. 23(3): 901–919.

Yu, S.Y., Zhang, J.X., Real, P.G.D., Zhao, X.L., Hou, K.J., and Gong, J.H., 2013a. The Grenvillian orogeny in the Altun-Qilian-North Qaidam mountain belts of northern Tibet Plateau: constraints from geochemical and zircon U–Pb age and Hf isotopic study of magmatic rocks. *Journal of Asian Earth Sciences*. 73: 372–395.

Zhang, A.D., Liu, L., Sun, Y., Chen, D.L., Wang, Y., and Luo, J.H., 2004. SHRIMP U-Pb dating of zircons and its geological significance from UHP granitoid gneiss in Altyn Tagh. *Chinese Science Bulletin*, 49(23): 2527 2532 (in Chinese).

Zhang, J.X., Li, H.K., Meng, F.C., Xiang, Z.Q., Yu, S.Y., and Li, J.P., 2011. Polyphase tectonothermal events recorded in metamorphic basement from the Altyn Tagh, the southeastern margin of the Tarim basin, western China: constraint from U-Pb zircon geochronology. *Acta Petrologica Sinica*, 27: 23–46 (in Chinese with English abstract).

Zhang, J.X., Mattinson, C.G., Meng, F.C., Wan, Y.S., and Tung, K., 2008. Polyphase ectonothermal history recorded in granulitized gneisses from the North Qaidam HP/UHP metamorphic terrane, Western China: Evidence from zircon U -Pb geochronology. *Geological Society of America Bulletin*, 120(5–6): 732–749.

Zhang, J.X., Zhang, Z.M., Xu, Z.Q., Yang, J.S., and Cui, J.W., 1999. The ages of U-Pb and Sm-Nd for eclogite from the western segment of Altyn Tagh tectonic belt. *Chinese Science Bulletin*, 44(24): 2256–2259.

Zhang, J.X., Zhang, Z.M., Xu, Z.Q., Yang, J.S., and Cui, J.W., 2001. Petrology and geochronology of eclogites from the western segment of the Altyn Tagh, northwestern China. *Lithos*, 56(2):187–206.

Zhao, Z.X., Wei, J.H., Fu, L.B., Liang, S.N., and Zhao, S.Q., 2017. The Early Paleozoic Xitieshan syn-collisional granite in the North Qaidam ultrahigh-pressure metamorphic belt, NW China: Petrogenesis and implications for continental crust growth. *Lithos*, 278–281: 140–152.

About the first author

CHEN Hongjie, male, born in 1985 in the city of Shangqiu, Henan Province; a Ph.D. candidate at the Institute of Geology, Chinese Academy of Geological Sciences, with major in mineralogy, petrology and mineral deposit geology.